Design of Quasi Crystal Based Broadband GHz Metasurface

By

Meraj E Mustafa

MS (EE)-8S
00000202364

Supervisor

Dr. Farooq Ahmad Tahir

The thesis submitted in partial fulfillment of the requirements for the degree

of Masters of Science in Electrical Engineering (MS EE)

at

Research Institute for Microwave and Millimeter-Wave Studies (RIMMS),
National University of Sciences and Technology (NUST),
Islamabad, Pakistan.

(January 2019)

Approval

It is certified that the contents and form of the thesis entitled “Design of Quasi Crystal Based Broadband GHz Metasurface” submitted by Meraj E Mustafa have been found satisfactory for the requirement of the degree.

Advisor: Dr. Farooq Ahmad Tahir

Signature: _____

Date: _____

Committee Member 1: Dr. Muhammad Umar Khan

Signature: _____

Date: _____

Committee Member 2: Dr. Nosherwan Shoaib

Signature: _____

Date: _____

Committee Member 3: Engr. Ahsan Azhar

Signature: _____

Date: _____

I dedicate this work to my parents, friends and teachers for their guidance and unconditional support throughout my career

Certificate of Originality

I hereby declare that this submission is my own work and to the best of my knowledge it contains no materials previously published or written by another person, nor material which to a substantial extent has been accepted for the award of any degree or diploma at NUST RIMMS or at any other educational institute, except where due acknowledgement has been made in the thesis. Any contribution made to the research by others, with whom I have worked at NUST RIMMS or elsewhere, is explicitly acknowledged in the thesis.

I also declare that the intellectual content of this thesis is the product of my own work, except for the assistance from others in the project's design and conception or in style, presentation and linguistics which has been acknowledged.

Author Name: Meraj E Mustafa

MS (EE)-8S
00000202364

Signature: _____

Acknowledgements

I am grateful to my supervisor Dr. Farooq Ahmad Tahir for his guidance, feedback and encouragement throughout my thesis. His constant support helped me to accomplish my goal. I am also thankful to Dr. Muhammad Umar Khan, Dr. Nosherwan Shoaib and Mr. Ahsan Azhar for being on my thesis guidance and evaluation committee. My thanks are expressed to Dr. Muhammad Amin and Dr. Omar Siddiqui from Taibah Engineering University, Saudi Arabia for their tremendous cooperation and useful discussions on metasurfaces. I would also like to thank all my colleagues at RIMMS, in particular Mr. Hidayatullah for assisting in performing the experiment.

Abstract

In this thesis, quasi-crystal metasurface based-on super-cell technique is designed to realize multiple operations at microwave frequencies. In this technique, distinct sized anisotropic patches are placed in one super cell to couple response of each patch operating in different frequency bands. Thus, the proposed design benefits from the individual resonant response of anisotropic patches and also from their coupled response due to periodic perturbations in the square lattice. The metasurface provides simultaneous half- and quarter-wave plate operations to transform linear to cross and linear to circular polarization conversions respectively. Such a broadband and multifunctional planar metasurface will help miniaturize the size of microwave systems whilst being ultrathin than the current reflective metasurface based polarizers. Furthermore, the physical dimensions of the super-cell are optimized to achieve high efficiency cross polarization conversion avoiding the stacking of multiple resonator layers upon each other.

In addition to the main contribution discussed above, the thesis also includes a comment on a published research paper in which a metasurface structure is falsely claimed as a perfect absorber. This proclaimed anisotropic metasurface was predominantly a cross polarizer for normally incident electromagnetic wave. Therefore, the use of this asymmetric structure is limited only to the applications where cross polarization operation is desired.

Table of Contents

List of Figures

List of Acronyms

EM	Electromagnetic
HWP	Half Wave Plate
QWP	Quarter Wave Plate
CST	Computer Simulation Technology
LHCP	Left Hand Circular Polarization
RHCP	Right Hand Circular Polarization

CHAPTER 1

Introduction

1.1 Polarization of Electromagnetic Wave

Electromagnetic (EM) waves are generated due to accelerated charges or time varying electric current. Electromagnetic waves are oscillations of electric and magnetic fields which are orthogonal to each other and orthogonal to the direction of propagation as well. Polarization is one of the important parameter of EM waves among other parameters like wavelength, phase, and frequency. Polarization is the time varying orientation of electric field vector at a fixed position in space [1]. Polarization state nature of electromagnetic waves influences the wave-matter interaction. Many applications such as optical sensing, satellite communications, reduction in radar cross section and contrast imaging microscopy are realized by controlling the orientation of polarization state of waves. Polarization plays an important role in the antennas for communication purpose. Linearly polarized antenna can receive and transmit EM waves in one direction; horizontal or vertical. Linearly polarized antenna in the receiving mode can only receive EM waves from the transmitting antenna of similar polarization. While, circularly polarized antenna has the advantage of receiving EM waves from either direction. There are three types of polarization that are discussed below.

A time-harmonic wave has linear polarization if the time varying electric or magnetic field vector is along the same straight line at a fixed position in space as shown in Fig. 1.1. A wave is considered to be linearly polarized if one of the following two conditions is fulfilled.

a) E_x or E_y

b) $E_x = E_y$ and $\Delta\Phi = \Phi_x - \Phi_y = n\pi$; where n is an integer.

Polarization of EM wave is mathematically represented in terms of Jones matrix. When EM wave is passed through any optical element, the polarization of the resultant wave is calculated from the product of Jones matrix of optical elements and Jones vector of the incident wave [2]. According to IEEE standard rule, polarization is always taken away from the observer.

$$\begin{pmatrix} E_x(z,t) \\ E_y(z,t) \end{pmatrix} = \begin{pmatrix} E_{ox}e^{i(kz-\omega t+\varphi_x)} \\ E_{oy}e^{i(kz-\omega t+\varphi_y)} \end{pmatrix} = \begin{pmatrix} E_{ox}e^{i\varphi_x} \\ E_{oy}e^{i\varphi_y} \end{pmatrix} e^{i(kz-\omega t)} \quad (1.1)$$

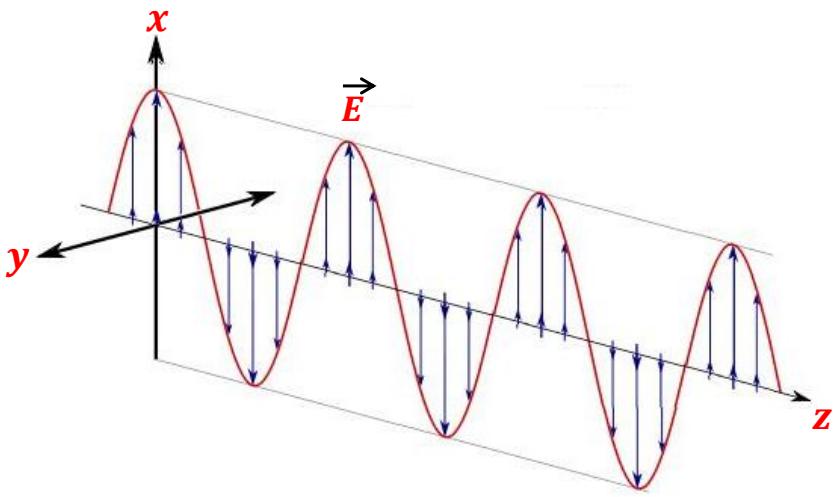

Figure 1.1: Linearly polarized wave [3]

Jones vector from Eq. 1 is given below.

$$\begin{pmatrix} E_{ox}e^{i\varphi_x} \\ E_{oy}e^{i\varphi_y} \end{pmatrix}$$

Jones vector shows the magnitude and phase of electric field in x and y directions. The normalized Jones vector in the horizontal and vertical directions is represented by $\begin{bmatrix} 1 \\ 0 \end{bmatrix}$ and $\begin{bmatrix} 0 \\ 1 \end{bmatrix}$ respectively.

A time-harmonic wave has circular polarization if the time varying electric or magnetic field vector's tip forms a circular locus at a fixed position in space. A circularly polarized wave must meet the following two conditions:

a) $E_x = E_y$

b) $\Delta\Phi = \Phi_x - \Phi_y = 90^0$

The rotational direction of circularly polarized wave is determined by revolving the phase-leading component towards the phase-lagging component when the wave travels away from the observer. Clockwise rotation will result in right-hand circularly polarized (RHCP) wave

and anticlockwise rotation will give left-hand circularly polarized (LHCP) wave as shown in Fig 1.2.

Jones vector for RHCP is represented in matrix form by:

$$\frac{1}{\sqrt{2}}\begin{bmatrix}1\\ j\end{bmatrix}$$

While, Jones vector for LHCP is denoted by:

$$\frac{1}{\sqrt{2}}\begin{bmatrix}1\\ -j\end{bmatrix}$$

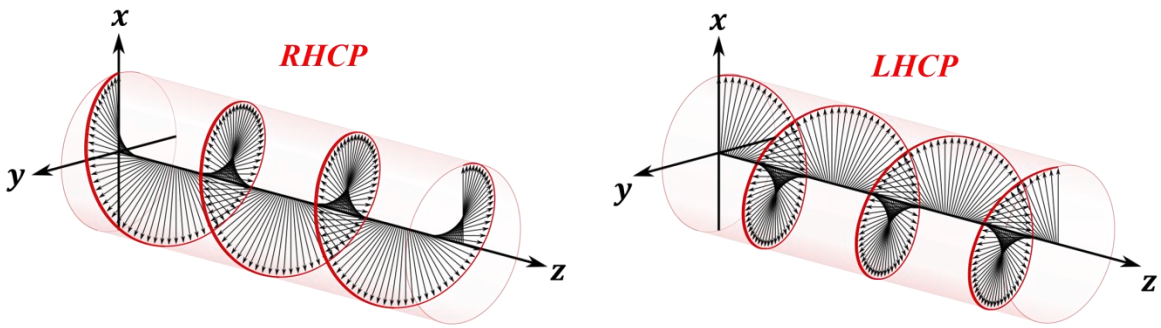

(a) (b)

Figure 1.2: (a) Right-hand circularly polarized wave (b) Left-hand circularly polarized wave [3]

A time-harmonic wave is regarded to be elliptically polarized if the tip of time varying electric field vector form a ellipse at a fixed location in space as shown in Fig 1.3. The wave is considered to be elliptically polarized if it is neither linearly polarized nor circularly polarized. The rule to find the sense of rotation of elliptical polarization is similar to the circular polarization.

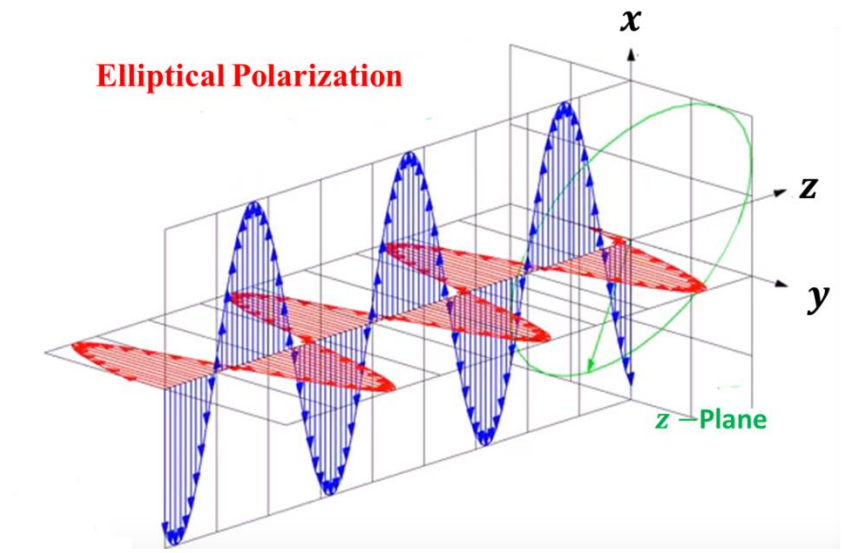

Figure 1.3: Illustration of Elliptical Polarization [4]

1.2 Research Motivation

1.2.1 Polarization Manipulation

Electric field vector in the EM waves is controlled and manipulated for the large scale applications at microwave and terahertz frequencies such as wireless communication. Traditional techniques are usually utilized for the polarization manipulation of EM wave which are given below:

- Faraday's Effect
- Birefringence in anisotropic crystals

Birefringence crystal can change the polarization state of EM by introducing the phase delay between the two components with different handedness. A linearly polarized wave can be dissolved in to two circularly polarized components of same magnitude but with opposite handedness. When the phase delay of 180^0 or half wavelength is introduced between the components, the resulting wave will be converted into its orthogonal components. This phenomenon is known as half wave plate (HWP). Similarly, when the phase of one linear component is delayed by 90^0 or quarter wavelength with respect to its orthogonal component of same magnitude, the resulting wave will be circularly polarized. This phenomenon is known as quarter wave plate (QWP). Faraday's effects works on the magneto-optical principle; that is

the interaction of the electromagnetic wave and magnetic field [5]. An external magnetic field which is excited using batteries is utilized for the polarization conversion of EM wave.

A few of the inherent disadvantages of these conventional techniques are given below.

(i) External batteries are required to excite the magnetic field in Faraday's effect
(ii) A Bulky structure at low frequency
(iii) Narrow-band
(iv) Polarization manipulation is sensitive to the oblique angles
(v) Incompatible with miniaturized polarization control devices

To cope with the disadvantages posed by these techniques for the manipulation of polarization state, researchers have introduced a new field of periodic artificial structures known as Metamaterials and Metasurfaces. These surfaces help in miniaturization of the whole optical and microwave systems because of their compactness and compatibility with the planar polarization control devices [6-9]. Multi-functionality is another important aspect that will be helpful to reduce the overall complexity of the system.

1.2.2 Metamaterials

Metamaterials are periodically repeating artificial structures possessing exceptional electromagnetic properties not found in natural materials [10-12] . Metamaterials do not derive their properties from their base materials such as metal and dielectric from which they are made. Metal and dielectric that make metamaterials have positive permittivity and permeability. Metamaterials are supported by metal-dielectric structures with specific geometry that couple electric field leading to negative refractive index due to simultaneous negative permittivity and permeability [13]. In 1968, theoretical idea of negative refractive index was first floated by Veselago [14]. Pendry in 1999 suggested the idea of negative permittivity and negative permeability by using cut-wire and split-ring resonators respectively [15]. Later in 2001, Shelby introduced negative refractive index metamaterials by simultaneously achieving negative permittivity and permeability using cut wires and Split-ring at microwave frequencies as shown in Fig 1.5 [16]. In this structure, cut wire is giving negative permittivity while split-ring is producing negative permeability in an overlapping frequency region.

Metamaterials are subwavelength unit cell structure with periodicity less than the operating wavelength containing electromagnetic properties that can be used in super lenses [17], invisibility cloaking [18], antennas [19] , absorbers [20] and bio-sensors [21].

Figure 1.4: Negative refractive index using cut wire and split-rings [16]

1.2.3 Metasurfaces

Metasurfaces are planar equivalent of three dimensional metamaterials with subwavelength unit cell size and thickness [22-24]. Compared to bulk metamaterials, propagation phase of metasurfaces is significantly reduced due to subwavelength thickness making the refractive index, permittivity and permeability irrelevant. In contrast, surface reflection and transmission are of special interest in metasurfaces. Subwavelength thickness causes low loss in metasurfaces when compared with 3D metamaterials due to minimal propagation phase. Metasurfaces are much easier to fabricate at micro- and nano-scale using lithography and nanoprinting methods. Due to the high potentials in applications, metasurfaces will dominate the metamaterials in the future as well.

Metasurfaces are engineered in such a way to control the amplitude, phase, direction of propagation, polarization state and shape of wavefront. Phase change is created using metasurface that alter the boundary conditions resulting in change of reflection and transmission coefficients. Metasurface based on the Pancharatnam-Berry phase are used in planar lens to converge or diverge the beam by controlling the handedness of circularly polarization [25]. A beam deflector based metasurface with high transmission efficiency of 86% is achieved by matching the surface impedance with air to minimize the reflections [26].

In recent years, a lot of work is theoretically and practically demonstrated to control the polarization of wave. Polarization state of wave remains same when the resonator (meta-atom) is highly symmetric. Breaking the symmetry leads to additional advantage of polarization change due to phase delay between the Eigen modes. This results in the polarization conversion of EM wave. Dielectric metasurfaces have also gained attention because of negligible Ohmic losses at optical frequency range [27].

Lastly, quasi-crystal based plasmonic metasurface in infrared and Terahertz frequency regime has induced interest among scientific community over the past decade. Generally, wave propagation can be controlled using classical bandgap technology at subwavelength scale [28-30]. Such bandgaps can be realized with the help of photonic crystals that are periodic dielectric materials in one, two, or three dimensions [31]. Nowadays, metasurface based on photonic crystals are altered to form quasi-crystal that offer the advantage of broadband operation [32-34]. Quasi-periodic unit cell are arranged to control wave propagation at sub-wavelength scale. The collective characteristics of such quasi-crystal based resonators depend upon the individual response of the each resonator. In this context, planar quasi-crystal metallic structures are used in light harvesting [35-37] and solar cell applications [38-40].

1.3 Thesis Contribution

In this thesis, quasi-crystal metasurface based on a novel technique is designed, fabricated and measured. This technique is usually used in the THz frequency regime to couple the response of each meta-atoms operating in different frequency bands. In this technique, different resonators are placed in one super cell on a single layer to couple the response of each resonator operating at different frequency bands instead of using multi-resonator layers to realize the broadband operation. In addition, this metasurface gives multifunctional operations, a simultaneous half-wave plate (HWP) and quarter-wave plate (QWP) operations, which is not easily realizable from conventional metasurfaces. Metasurface is also optimized here in such a way to give high efficiency wideband cross-polarization. In the end, idea is tested and experimental results validate the simulation results. Such a broadband ultrathin and multifunctional planar metasurface will help miniaturize the size of optical and microwave systems. The proposed idea is helpful for the potential applications of reflector antennas, remote sensing and control of radar cross-section.

1.4 Thesis Organization

The thesis is organized as follows:

- **Chapter 1** includes the overview of polarization of electromagnetic wave, motivation behind selection of the topic and thesis contribution in the field of metasurfaces.
- **Chapter 2** gives the detailed literature review of the research work carried out in metasurfaces.
- **Chapter 3** presents the novel design of quasi-crystal metasurface that can simultaneously work as a cross-polarizer and circular polarizer. The aforementioned technique takes advantage from individual response of anisotropic patches and the coupled response from multiple patches in super-cell. Simulation results are in good match with the experimental result which validates the presented concept.
- **Chapter 4** discusses the comment on a published research papers in which a metasurface polarizer is falsely claimed as a perfect absorber.
- **Chapter 5** concludes the thesis and gives probable extension of the presented work in the future.

CHAPTER 2

Literature Review of Metasurfaces

In this chapter, various types of polarization conversion metasurfaces that have obvious advantages over conventional techniques are discussed.

2.1 HWP Metasurfaces

In this section, manifold published designs of linear to cross polarization conversion or HWP metasurfaces are discussed in detail. Cross Polarization metasurfaces rotate the linearly polarized component of wave into its orthogonal component. The operation of cross conversion can be achieved in both reflection [41-43] and transmission mode [44,45] . In reflection mode, an impinging x-polarized wave is converted into its y-polarized component or vice versa when reflected after normally striking the metasurface. A ground plane is usually inserted in reflection mode structures at the bottom of the substrate to reflect all incident energy of the incoming wave. In the transmission mode, linear polarization is rotated into its cross polarization when received after passing through the metasurface. Anisotropic configuration of the unit cell is the necessary condition for the polarization conversion of impinging wave. Anisotropic structures do not look similar when broken along x, y and x-y plane.

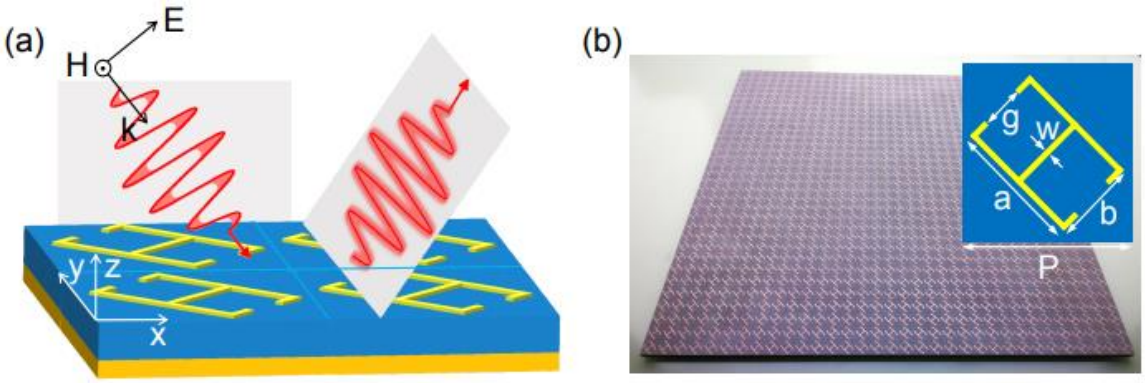

Figure 2.1: (a) Schematic of proposed polarization convertor (b) Fabricated sample [43]

A reflective 45^0 angular stable polarization convertor metasurface based on the split ring resonators is proposed in the literature which converts linear polarization in to its cross-polarization in the frequency band of 5-10.8 GHz [41]. The main drawback of the aforementioned metasurface is reduced conversion efficiency with the increase in oblique angle of the wave. Another anisotropic double V-shaped cross polarizer has achieved the ultrawide bandwidth from 12.4 to 27.96 GHz with an average polarization conversion ratio above 90% [42]. A single V-shape resonator is responsible for two resonances in the structure due to generation of symmetric and antisymmetric modes. However, bandwidth of the designed metasurface is significantly reduced with the increase in incident angle. Anisotropy in the unit cell results in the cross polarization conversion by introducing the phase delay of 180^0 between two Eigen mode polarizations, u- and v-polarizations.

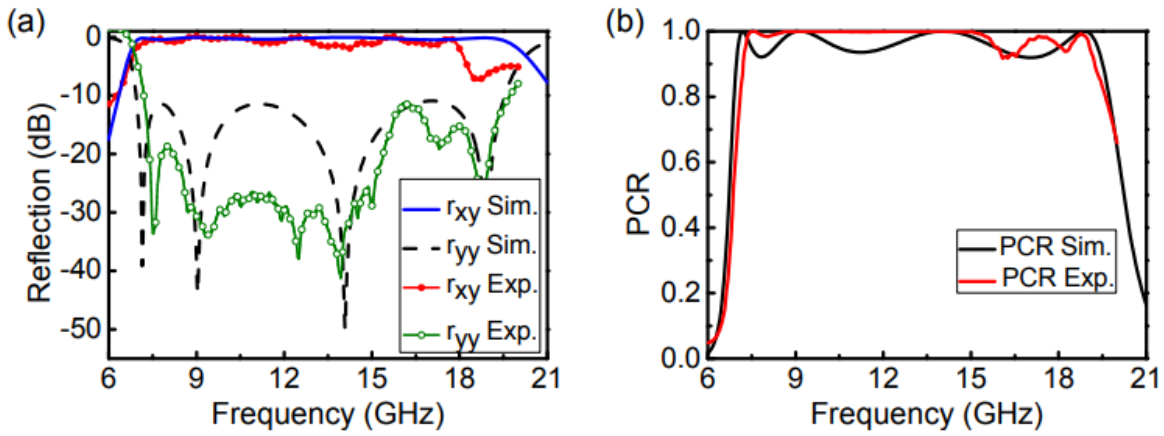

Figure 2.2: (a) Simulated and experimental reflection spectra of the proposed metasurface (b) Polarization conversion rate (PCR) [43]

In [43], a reflective high efficiency periodically repeating H-shaped unit cell is fabricated and the schematic can be seen from Fig. 2.1. The ground plane at the bottom results in no transmission of the incident electric field. The designed metasurface acts as 90^0 polarization convertor in the band of 7 to 19.5 GHz with polarization conversion efficiency (PCR) above 90% as shown in Fig. 2.2. Angular stability analysis of the designed metasurface indicates the average PCR above 80% for the incident angle approaching 41.5^0. Four electromagnetic resonances generated in the metasurface are the reason behind broadband polarization conversion with relative bandwidth of 94%.

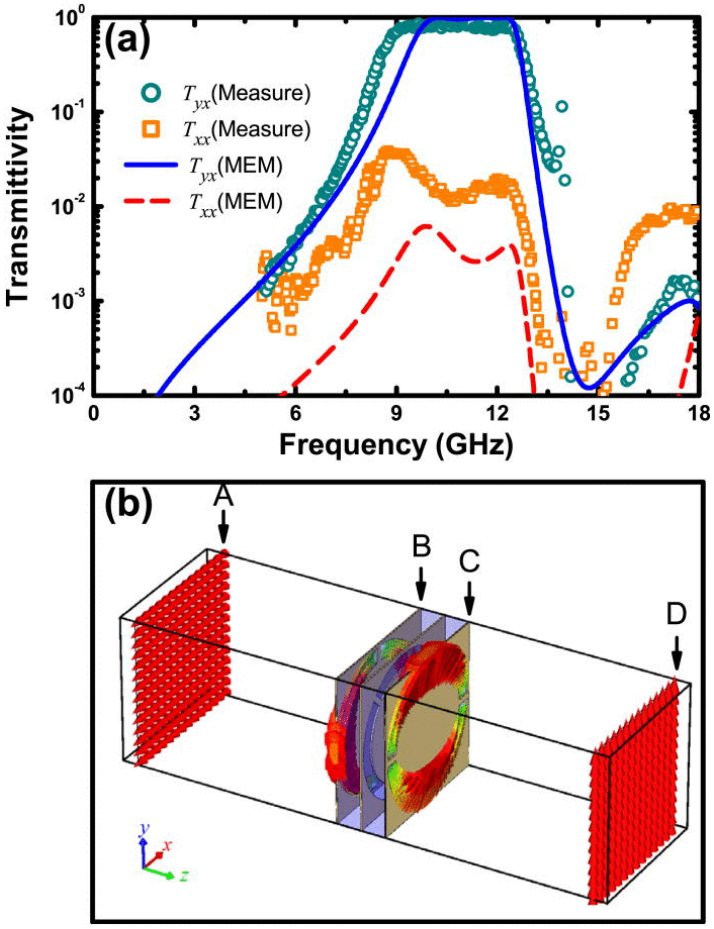

Figure 2.3: (a) Calculated and measured transmission spectra (b) Spatial distribution of electric field in x-direction and resulting slice D is showing polarization rotation in y-direction [44]

Similarly, a multilayer wideband polarization conversion metasurface is designed that works in transmission mode from 9.8 GHz to 12.5 GHz. The efficiency of the designed metasurface is 96%, covering the fractional bandwidth of 24%. The proposed structure is composed of tri-layer split-ring resonators for broadband polarization conversion as shown in Fig. 2.3(b) [44]

Chiral metasurfaces usually consist of bilayer or multilayer structure utilized for polarization rotation by coupling the electric and magnetic fields. The mirror image of the chiral structures does not perfectly overlap on its original structure. One of the chiral metasurfaces containing three layers is published in the literature that gives strong cross-polarization conversion in multi-bands. Top and bottom layers of the structure are composed of double-split rings with bottom layer 90^0 rotated with respect to top layer. To introduce the chirality and break the symmetry of top and bottom layer, a grating layer is also inserted as a

middle layer with a 45^0 rotation angle with respect to y-axis. Asymmetric transmission effect is an important property of these types of metasurfaces, resulting in maximum cross-polarization transmission in different frequency bands for x- and y-polarized forward propagating wave, see Fig. 2.4. [45]

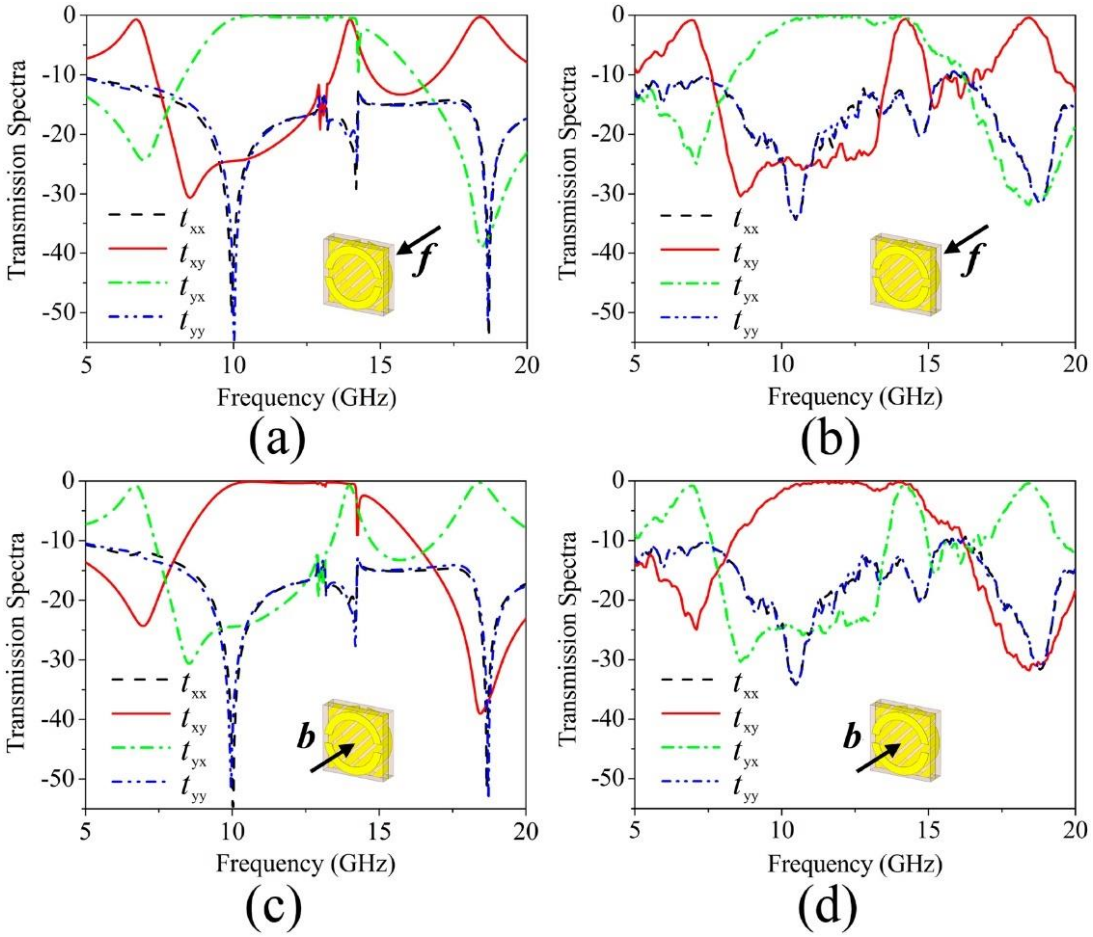

Figure 2.4: Transmission coefficients for the forward (a) and (b) and backward (c) and (d) propagating waves [45]

2.2 QWP Metasurfaces

This section gives an overview of the circular polarization conversion or QWP metasurfaces. Circular polarization conversion metasurfaces convert the linearly polarized wave into circular polarization by reflecting or transmitting the co- and cross-polarized components with same magnitude and phase difference of $\pm 90^0$. The sign of phase difference between co- and cross-component gives the handedness of circularly polarized wave. The formation of right and left hand circularly polarized wave is due to the phase difference of 90^0 and -90^0 respectively. In

general, anisotropic and chiral metasurfaces are utilized for the circular polarization conversion of incident waves [46-48].

In [46], a dual band circular polarization metamaterial is designed using dual square array of novel asymmetric unit cell. The asymmetric nature of the unit cell causes strong chirality; coupling of electric and magnetic field that result in circular polarization conversion. Simulation and measurement results confirm the formation of LHCP at 7.68 GHz and RHCP at 8.82 GHz, see Fig. 2.5.

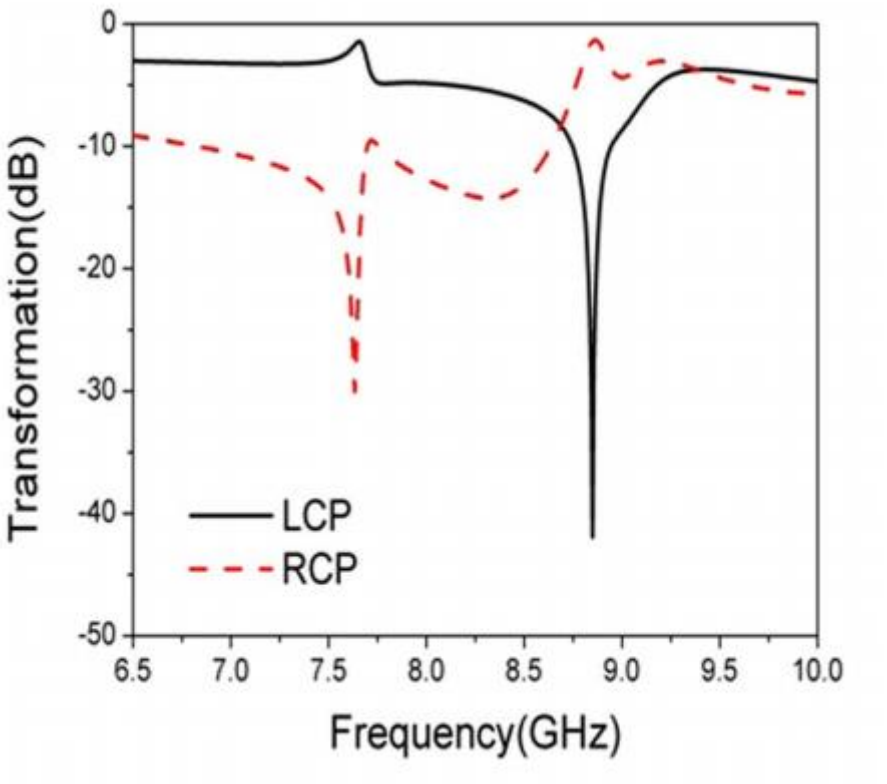

Figure 2.5: Transformation coefficients for y-polarized wave showing LCP and RCP [46]

One of the transmissive metasurfaces reported in the literature employs the anisotropic unit cell to achieve the circularly polarized wave. The design contains three corner truncated square patches surrounded by square loop apertures and separated by two dielectric substrates. Simulation results show the fractional bandwidth of 40.4% from 12.21 GHz to 18.39 GHz [47].

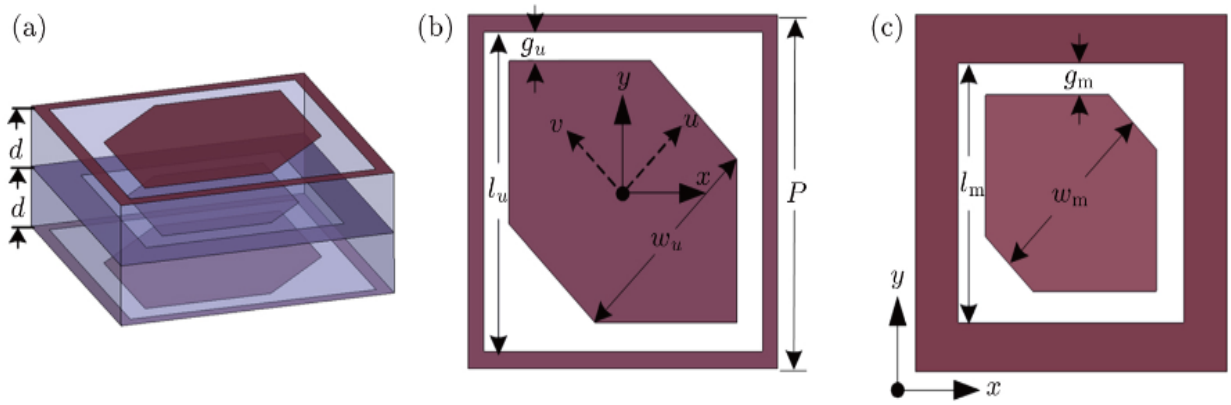

Figure 2.6: Unit cell of the proposed Metasurface (a) 3D view (b) Top and bottom layers (c) Middle layer [47]

Similarly, another reflective anisotropic metasurface containing Jerusalem cross with splits is designed, which can convert linearly polarized wave into the circularly polarized wave from 12.4 GHz to 21 GHz [48]. Two narrow slits are placed on the horizontal arm to maintain the 90^0 phase and broaden the bandwidth of the circular polarization. Horizontal I-shaped arm has the capacitive effect while vertical arm has inductive effect resulting in 90^0 phase difference over the whole operational bandwidth. The schematic illustration of linear to circular polarization conversion of wave is shown in Fig. 2.7.

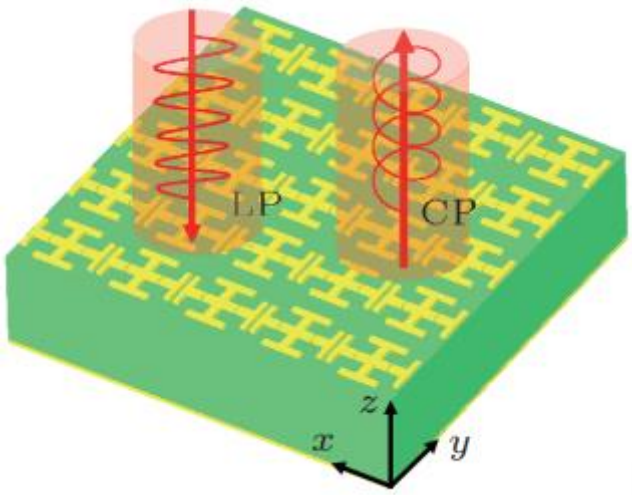

Figure 2.7: Illustration of linear-to-circular polarization conversion [48]

2.3 Metasurfaces for Simultaneous HWP and QWP Operations

Contrary to section 2.1 and 2.2, a simultaneous HWP and QWP metasurface can give both linear to cross and linear to circular polarization conversion in different frequency bands in both transmission and reflection mode. A few simultaneous HWP and QWP structures have been reported in the literature that are either multilayered or narrowband [49, 50].

In [49], a reflective dual layer metasurface patterned with L shaped metallic structure is demonstrated. The metasurface is regarded as QWP that can convert linear polarization to circular polarization in the dual frequency bands of 9.1 – 16.5 GHz and 20 – 25.4 GHz. In addition, simultaneous HWP operation is achieved in the frequency band of 17.4 to 18.9 GHz. The designed metasurface is also 30^0 angular stable for both x- and y-polarized waves. The novel aspect of the structure is its ability to give both LHCP and RHCP in different frequency bands. Simulation and measured results fairly match each other as shown in Fig. 2.9.

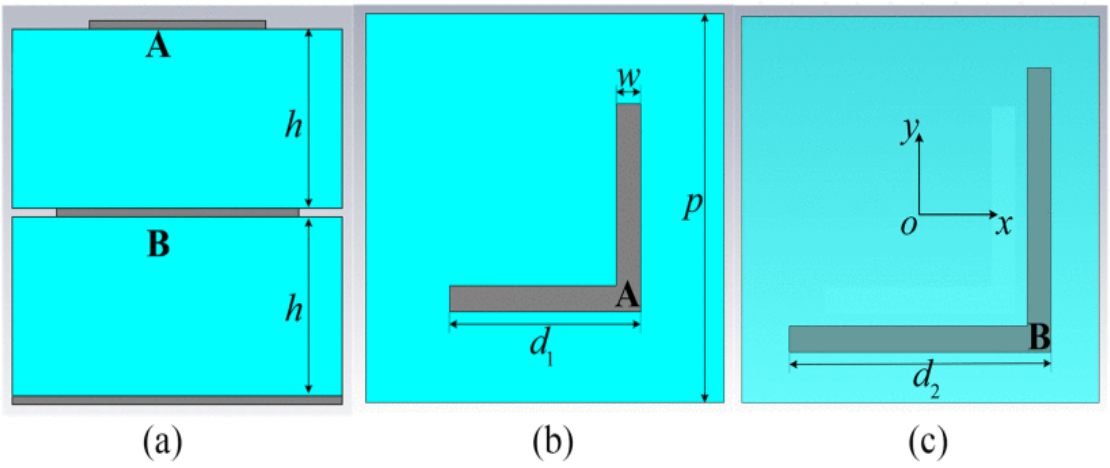

Figure 2.8: (a) Unit cell side view (b) Top layer (c) Bottom layer [49]

Similarly, a bilayer anisotropic metasurface is fabricated which exhibits narrowband simultaneous HWP and QWP operation in transmission mode. The top layer of unit cell is composed of square split ring resonator with a loop inside. Same pattern is made on the bottom side with 180^0 rotation to achieve the polarization conversion of the incident fields. Moreover, the QWP operation is quite stable to the variation in incidence angle [50]. The schematic diagram showing multifunctional operations is given in Fig. 2.10 (a).

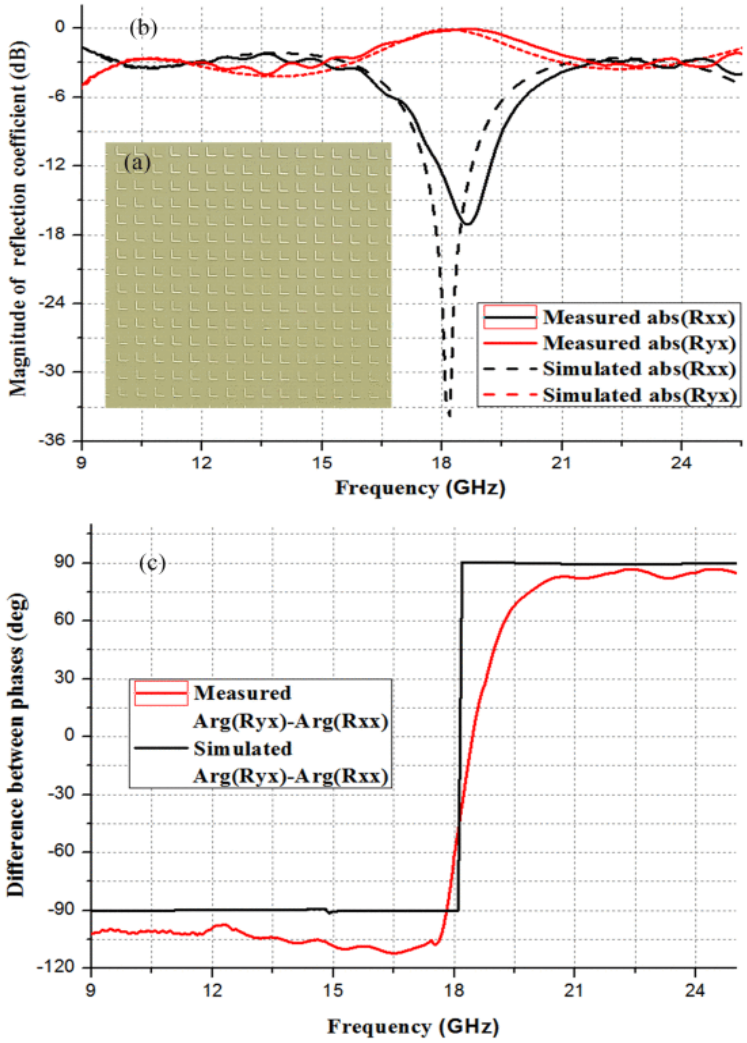

Figure 2.9: (a) Fabricated sample (b) Reflection coefficients (c) Phase difference between reflection coefficients [49]

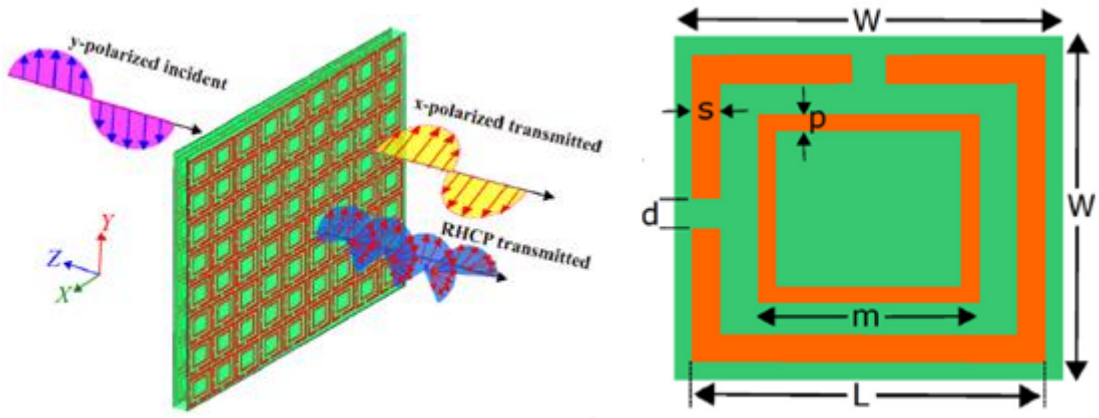

(a) (b)

Figure 2.10: (a) Schematic diagram (b) Top layer with geometric dimensions [50]

2.4 Conclusion

In summary, cross and circular polarization conversions have been achieved in the literature both in reflection and transmission mode. Anisotropic and chiral geometries of unit cells are employed to realize the polarization conversion from the metasurfaces. Furthermore, most of the researchers focused on the improvement of efficiency, bandwidth and unit cell size. It can be concluded from the literature review:

- Most of the design gives high efficiency polarization conversion by utilizing the multilayer structures.
- Single functionality such as HWP or QWP operation has been achieved in manifold designs.
- A few multifunctional metasurfaces are reported that give simultaneous HWP and QWP. Multi-functions are achieved at very narrowband of frequencies using single layer metasurface or broadband multifunction operations are realized with the help of multilayer structures.

CHAPTER 3

Metasurface Design

In this chapter, a novel concept employing super cell is implemented to achieve the simultaneous half- and quarter-wave plate operations by coupling the response of individual unit cells. The detailed design procedure with the analysis of results is discussed in this chapter.

3.1 Design Approach

In the design procedure of quasi crystal metasurface, a complete circular patch was simulated and analyzed at the first step. As seen in Fig. 3.1, no cross-polarization was seen because of the isotropic nature of the circular patch. Anisotropy was then deliberately introduced by putting a small square cut at top left corner of the circular element as shown in the inset of Fig. 3.2.

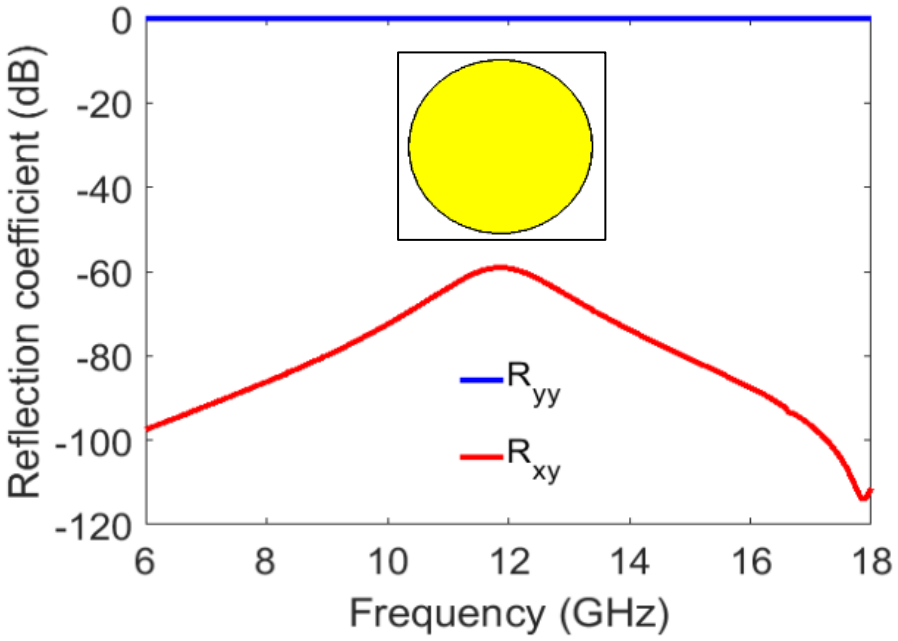

Figure 3.1: Reflection coefficients of isotropic circular patch

Owing to this anisotropy, the desired HWP and QWP operation is achieved at different frequency bands. Then, through full-wave simulations the parameter "d" is optimized to get maximum cross-polarization bandwidth. Similarly, another similar but relatively small patch is optimized using same parameters to get an efficient cross-polarization bandwidth relatively at higher frequencies. Finally, both anisotropic elements are placed in the square lattice making a supercell of size 2×2. The supercell is then briefly optimized to refine simultaneous HWP and QWP operation over wide frequency bands.

3.1.1 Large Patch Optimization

HWP or cross-polarizer converts linearly or circularly polarized incident waves into its corresponding cross-polarized components upon reflection from the metasurface. The relation between linearly polarized incident and reflected fields is established with Jones reflection matrix in Cartesian basis. Consider E_{xi} and E_{yi} as incident electric field components in x and y directions respectively. Similarly, consider E_{xr} and E_{yr} as reflected electric field components in x and y directions respectively.

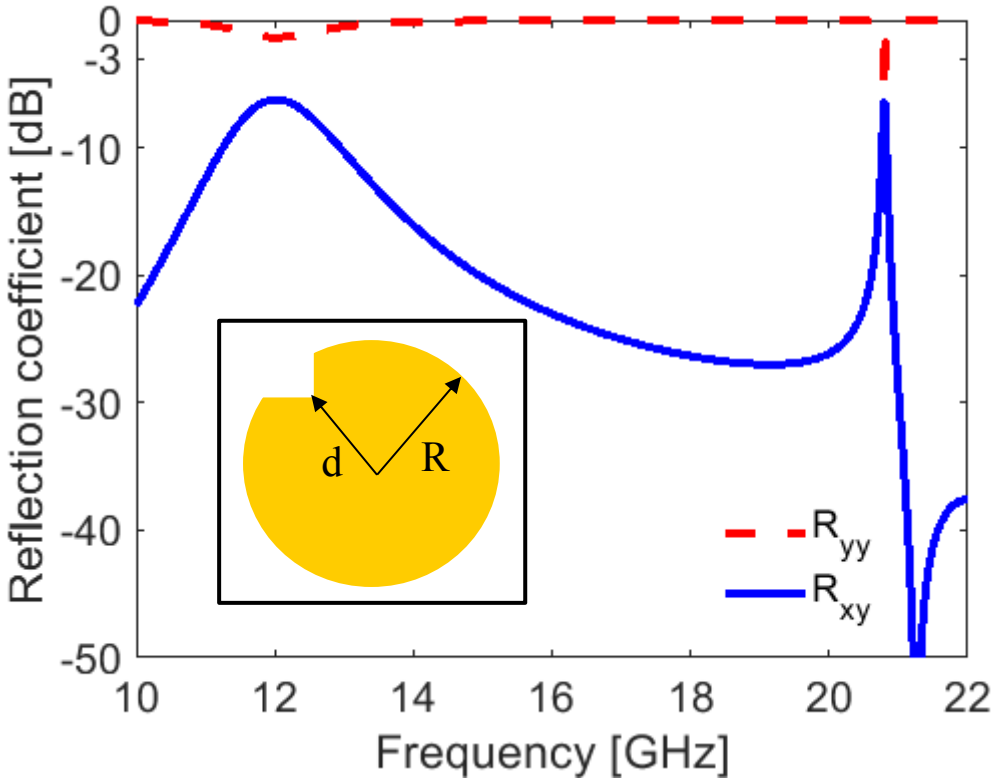

Figure 3.2: Reflection coefficients of large circular patch with d = 2.82 mm

$$\begin{bmatrix} E_{xr} \\ E_{yr} \end{bmatrix} = \begin{bmatrix} R_{xx} & R_{xy} \\ R_{yx} & R_{yy} \end{bmatrix} \begin{bmatrix} E_{xi} \\ E_{yi} \end{bmatrix} \quad (3.1)$$

Here, R_{xx}= $|E_{xr}|/|E_{xi}|$ and R_{yy}= $|E_{yr}|/|E_{yi}|$ are the co-polarized reflection coefficients for x and y-polarized incident waves respectively. While, R_{yx}= $|E_{yr}|/|E_{xi}|$ and, R_{xy}= $|E_{xr}|/|E_{yi}|$ are the cross-polarized reflection coefficients for x- and y-polarized incident waves respectively.

The radius of circular patch in unit cell is "R = 4 mm" with a square cut at its top left corner ($\theta = 45^0$) shown by diagonal distance "d". The period of unit cell is "p/2 = 10 mm" as shown in inset of Fig. 3.2. The metasurface layer and ground plane are distanced apart by a Rogers 5880 substrate with relative permittivity and loss tangent of 2.2 and 0.00009 S/m respectively. Large circular patch is optimized here for the -3 dB cross-polarization (R_{xy}) criterion to achieve the maximum bandwidth. For d = 2.82 mm in Fig. 3.2, It can be observed that R_{xy} starting to increase due to the creation of square cut at the top left corner but still remains well below -3 dB over the whole bandwidth resulting in poor cross-polarization conversion.

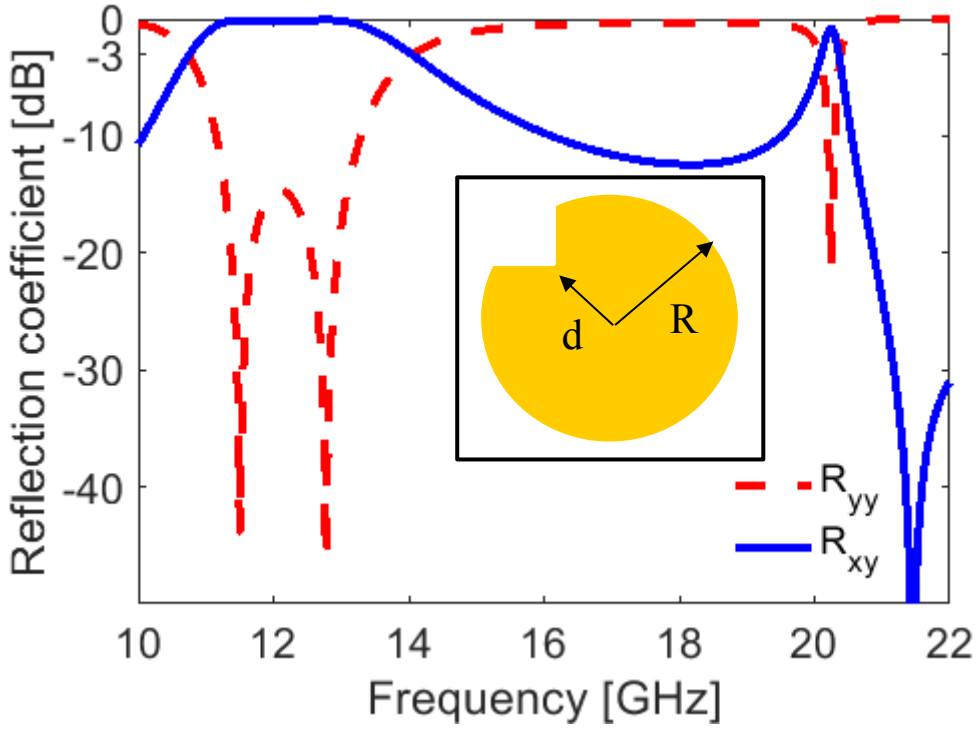

Figure 3.3: Reflection coefficients of large circular patch with d = 1.414 mm

Keeping the same radius R = 4 mm, diagonal distance "d" is optimized further to generate the resonances in the structure. It can be noted from Fig. 3.3, R_{xy} is above -3 dB from 11 GHz to 14 GHz when d = 1.414 mm. Large patch is behaving as an inductor and square cut is introduced to generate the capacitance in the structure. The combination of capacitance and inductance generated in the structure results in multiple resonances and thus increase in the bandwidth of the structure. The case of only y-polarized incidence is taken here because the response of the structure is same for x-polarized wave due to the mirror symmetry along v-axis.

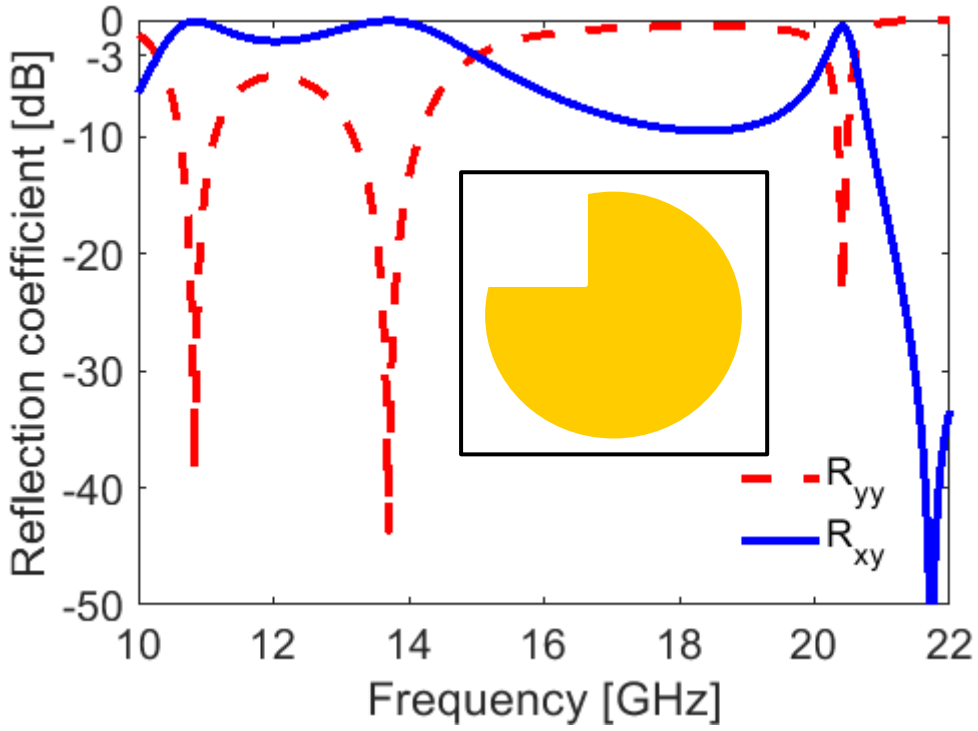

Figure 3.4: Reflection coefficients of large circular patch with d = 0.707 mm

Now, the size of the square cut is further increased to enhance the cross-polarization bandwidth. For d = 0.707mm, R_{xy} remains above -3 dB in the frequency band of 10.3 – 15 GHz. It is interesting to examine from Fig 3.4 that maximum cross polarization bandwidth is achieved. Furthermore, triple bands are achieved when the square cut is further increased with diagonal distance is kept zero. It is clear from the Fig 3.5. that multiple HWP bands are realized with radius R = 4 mm. Anisotropy has caused phase delay between two eigen mode polarizations u and v due to introduction of the square cut at the top left corner.

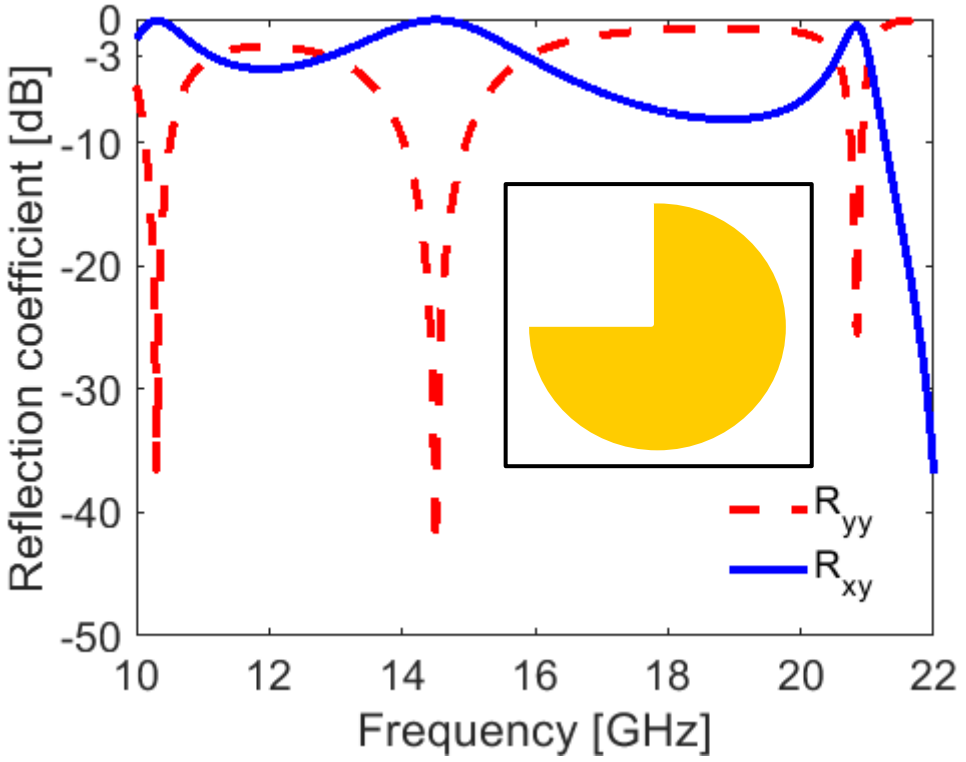

Figure 3.5: Reflection coefficients of large circular patch with d = 0 mm

3.1.2 Small Patch Optimization

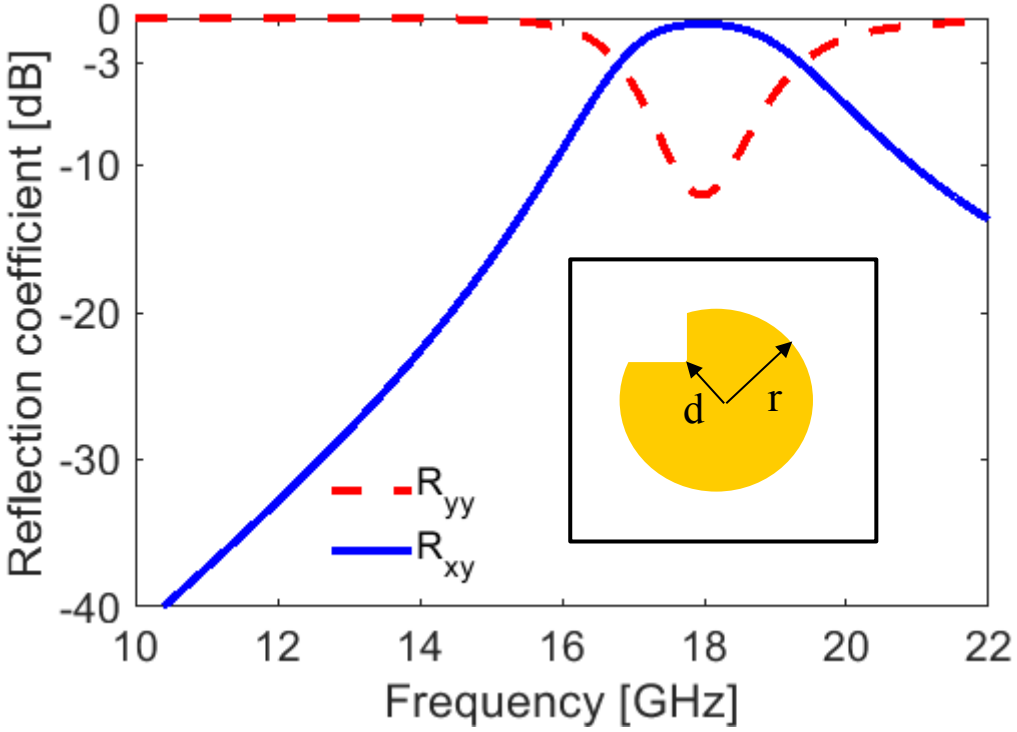

Figure 3.6: Reflection coefficients of small circular patch with d = 1.414 mm

Similarly, another small circular patch with radius r = 2.8 mm is optimized which is resonating at high frequencies to cover the frequency band gap from 15 to 20 GHz. As shown in Fig 3.6, a small square cut with d = 1.414 mm results in cross polarization conversion but with smaller bandwidth. A square cut introduces capacitance in the structure and combination of both capacitance and inductance generates the resonance frequency as shown in above figure. Cross-polarization bandwidth increases with the decrease in the diagonal distance. Fig. 3.8 shows that dual band cross polarization is achieved when d = 0 mm. So, the optimized diagonal distance "d" of both the large and small circular patch comes out to be 0.707 mm.

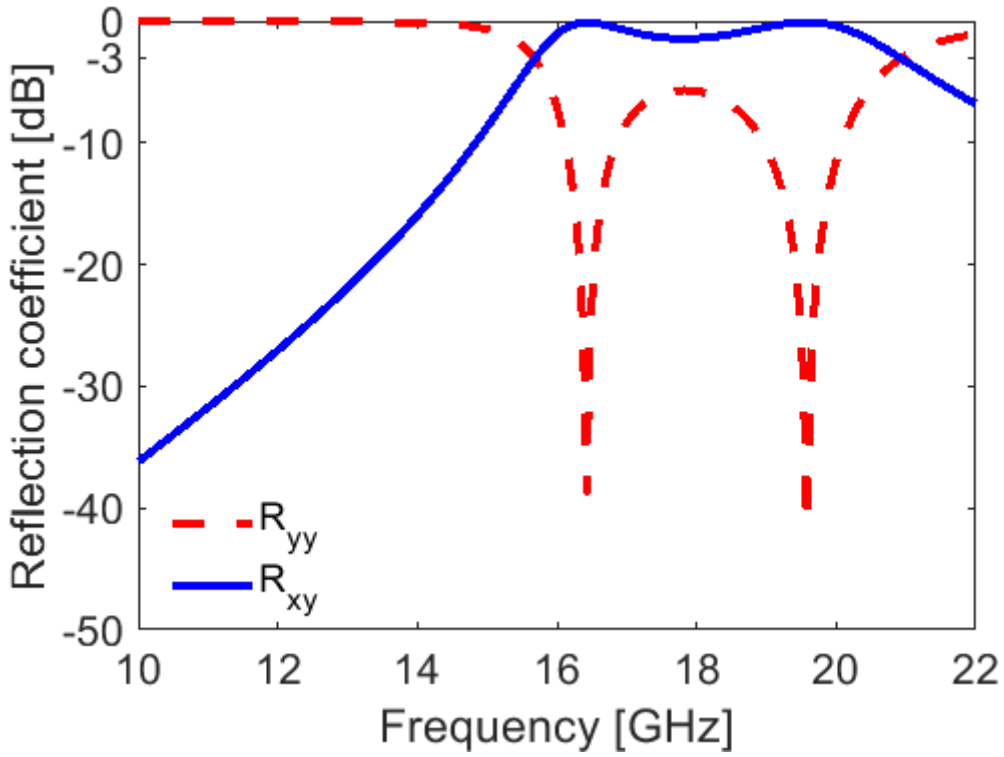

Figure 3.7: Reflection coefficients of small circular patch with d = 0.707 mm

3.1.3 Super-cell Composition

Now, to benefit from the supported resonance bands from these small and large sized patches simultaneously, a super cell is made by incorporating the varied sized anisotropic small and large sized patches. The modified periodic array each containing four patches/unit cells constitute the super cell. The small patches of radius r =2.85 mm are situated along the diagonal, whereas the large patches of radius R = 4.2 mm are located along anti-diagonal as shown in Fig. 3.9. Hence, the variation in size of patches adds periodic resonant perturbations

in both x- and y-directions. The metallic quasi-crystals under square lattice (i.e., periodic array of 2×2 super cell size) offer unique polarization insensitive characteristics under normal incidence as identical patches are placed along the diagonal of super cell. The optimized parameters are d=0.707 mm, θ =45^0, h=1.58 mm, and R=4.2 mm/2.85 mm for large and small patch respectively.

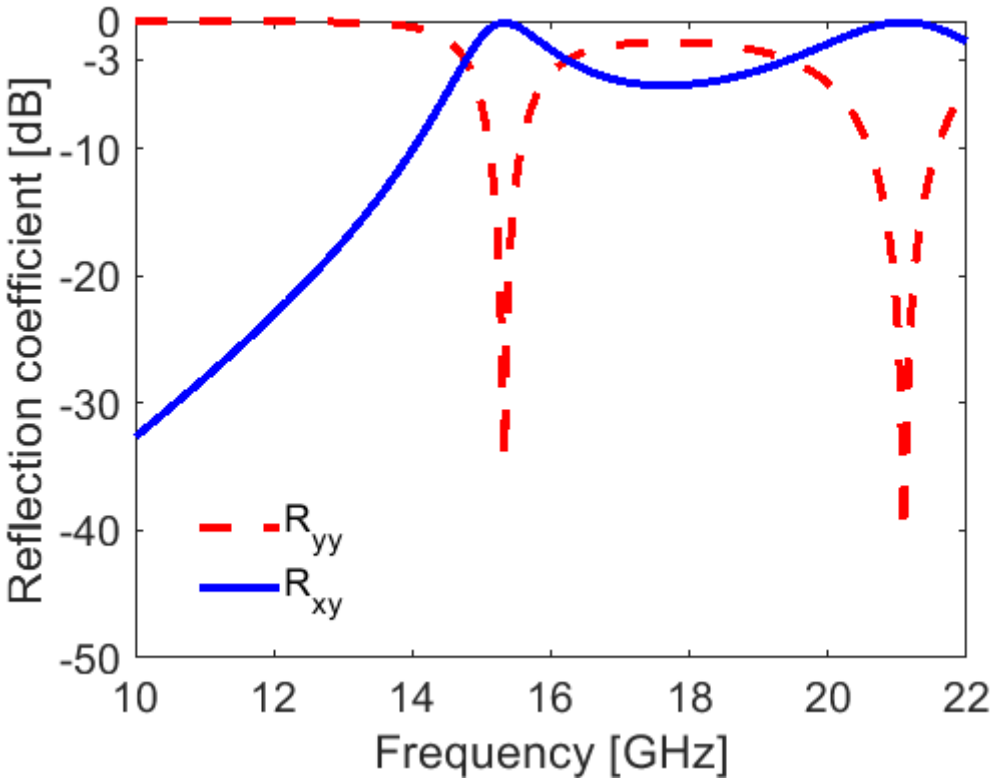

Figure 3.8: Reflection coefficients of small circular patch with d = 0 mm

The design consists of super cell of four anisotropic metallic patches as shown in Fig. 3.9. The radius of each circular patch in the square lattice is "R" with a square cut at its top left corner (θ =45^0) shown by diagonal distance "d". The period of unit cell is "p/2" as shown in inset of Fig. 3.9. The super cell is a collection of four unit cells that incorporate larger area. The period of super cell is denoted as "p". The metasurface layer and ground plane are distanced apart by a Rogers 5880 substrate with relative permittivity and loss tangent of 2.2 and 0.00009 S/m respectively. The geometrical parameters defined in Fig. 3.9 for anisotropic patch are θ =45^0 and d=0.707 mm unless stated otherwise. The period of super- and unit- cell is p=20 mm and p/2=10 mm respectively.

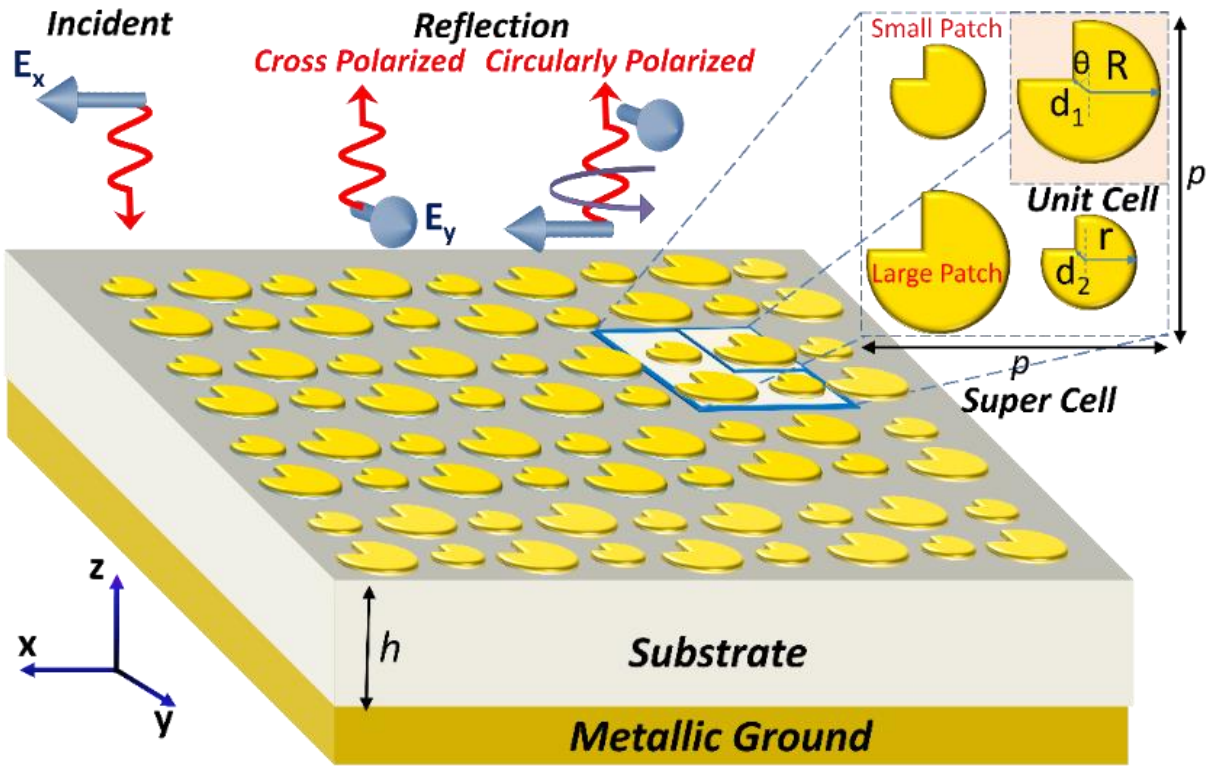

Figure 3.9: Schematic illustration of quasi-crystal metasurface

3.2 Results and Discussions

First, i find out the optimized response of individual unit cell without perturbations. Fig. 3.10(a) and Fig. 3.10(b) show the response of co- and cross-polarized reflection spectrum for two differently sized larger and smaller patch that are already optimized. As discussed above, the smaller patch of radius r = 2.85 mm is resonating at higher frequencies of 16.4 GHz and 19.5 GHz while large patch of radius R = 4.2 mm is resonating at lower frequencies of 10.8 GHz, 13.7 GHz and 20.4 GHz.

At resonance frequencies the co-polarized reflection coefficient for large patch reduces to -38 dB, -44 dB and -23 dB correspondingly increasing cross-polarization component R_{xy}. Similarly, the co-polarized reflection coefficient R_{yy} for small patch reaches -39 dB and -41 dB as shown in Fig. 3.10. Considering 3 dB bandwidth criterion for cross-polarization, two distinct non-overlapping bands i.e., 10.3 GHz - 15 GHz and 15.6 GHz - 20 GHz are supported by large and small patch metasurfaces respectively.

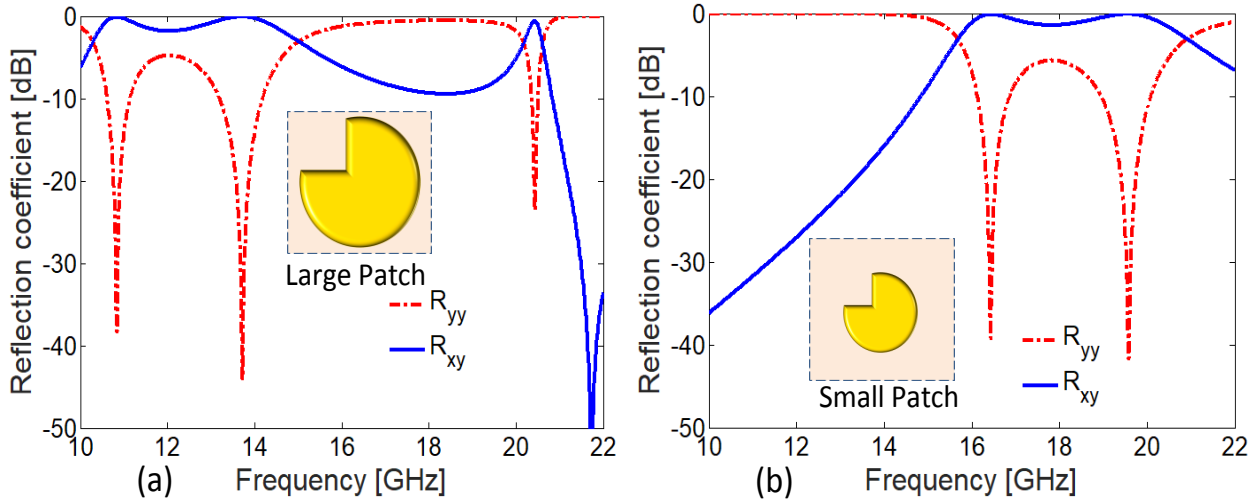

Figure 3.10: (a) Reflections from unit cell with large patch (b) Reflections from unit cell of small patch

Fig. 3.11(a)-(b) shows reflection spectrum for anisotropic quasi-crystal structure for both x- and y- polarized incident waves. Half wave plate operation is achieved for two broad frequency bands between 10.28 GHz - 15.50 GHz and 16.21 GHz - 18.80 GHz under normal incidence as shown in Fig. 3.11(a)-(b). It should be noted that the co-polarization coefficients R_{xx} and R_{yy} doesn't exceed a level of -3 dB throughout the bandwidth. It should also be noted that the response of quasi-crystal metasurface is nearly polarization insensitive and the minor difference is due to asymmetric location of square cut with reference to composition of supercell.

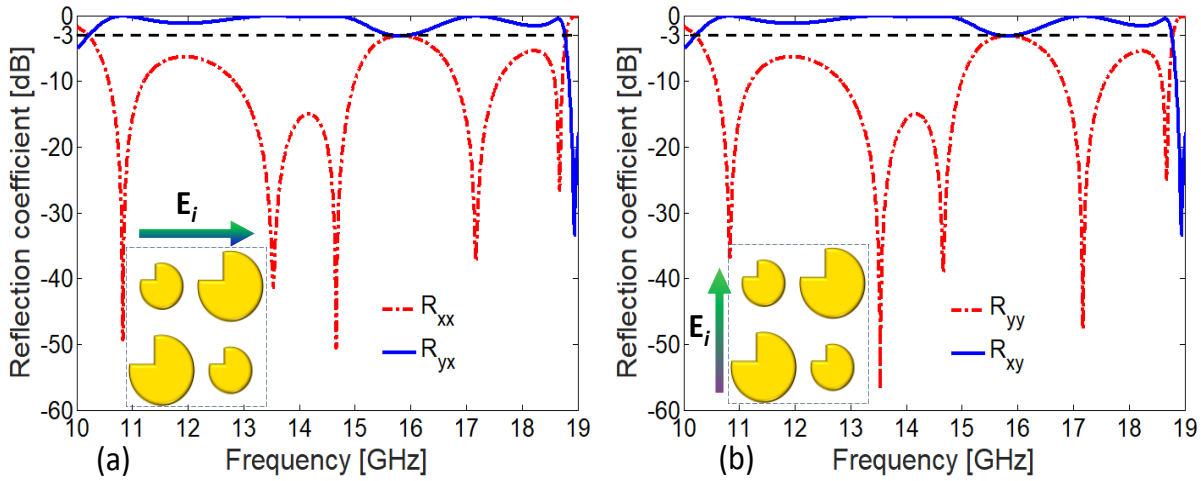

Figure 3.11: Co- and cross-polarized reflection components for super cell (a) x-polarized (b) y-polarized incident wave.

The proposed metasurface in Fig. 3.11(a)-(b) can also be simultaneously used as high efficiency circular polarizer. QWP or circular polarizer converts linearly polarized incident wave into circularly polarized wave and vice versa upon reflection from the metasurface. The relation between linearly polarized incident and circularly polarized reflected fields with corresponding Jones matrix in circular basis is established below. E_{+r} and E_{-r} as right-handed circular polarized (RHCP) and left-handed circular polarized (LHCP) reflected electric field components respectively.

$$\begin{bmatrix} \boldsymbol{E_{+r}} \\ \boldsymbol{E_{-r}} \end{bmatrix} = \begin{bmatrix} \boldsymbol{R_{+x}} & \boldsymbol{R_{+y}} \\ \boldsymbol{R_{-x}} & \boldsymbol{R_{-y}} \end{bmatrix} \begin{bmatrix} \boldsymbol{E_{xi}} \\ \boldsymbol{E_{yi}} \end{bmatrix} = \boldsymbol{R_{cl}} \begin{bmatrix} \boldsymbol{E_{xi}} \\ \boldsymbol{E_{yi}} \end{bmatrix} \tag{3.2}$$

The elements in matrix R_{cl} can also be converted to Cartesian basis as follows.

$$\begin{bmatrix} \boldsymbol{E_{+r}} \\ \boldsymbol{E_{-r}} \end{bmatrix} = \begin{bmatrix} \boldsymbol{E_{xr} + jE_{yr}} \\ \boldsymbol{E_{xr} - jE_{yr}} \end{bmatrix} = \frac{1}{\sqrt{2}} \begin{bmatrix} \boldsymbol{R_{xx} + iR_{yx}} & \boldsymbol{R_{xy} + iR_{yy}} \\ \boldsymbol{R_{xx} - iR_{yx}} & \boldsymbol{R_{xy} - iR_{yy}} \end{bmatrix} \begin{bmatrix} \boldsymbol{E_{xi}} \\ \boldsymbol{E_{yi}} \end{bmatrix} \tag{3.3}$$

The elements in Jones matrix R_{cl} demonstrate the ability of the structure to convert linearly polarized incident fields i.e., E_{xi} and E_{yi} to circularly polarized reflected fields i.e., . E_{+r} and E_{-r}. Here, subscripts "+" and "—" represents right-handed and left-handed waves respectively. Scaling factor of $\frac{1}{\sqrt{2}}$ normalizes the reflected electric field vector between 0–1 and also satisfies the passivity constraint.

Figure 3.12(a) shows that reflection components R_{yy} and R_{xy} have nearly same magnitude (R_{xy}/R_{yy}= 1) and a phase difference of 270^0 in the frequency range of 15.51 GHz –16.20 GHz, see Fig. 3.12(b). The condition for circular polarization is also met at narrow band around 10.15 GHz – 10.27 GHz. It is worth mentioning that the two frequency bands offer near ideal circular polarization conversion. These ideal characteristics are attributed to negligible loss in the substrate, equal power distribution and $\pm 90^0$ phase difference between two orthogonal reflection components.

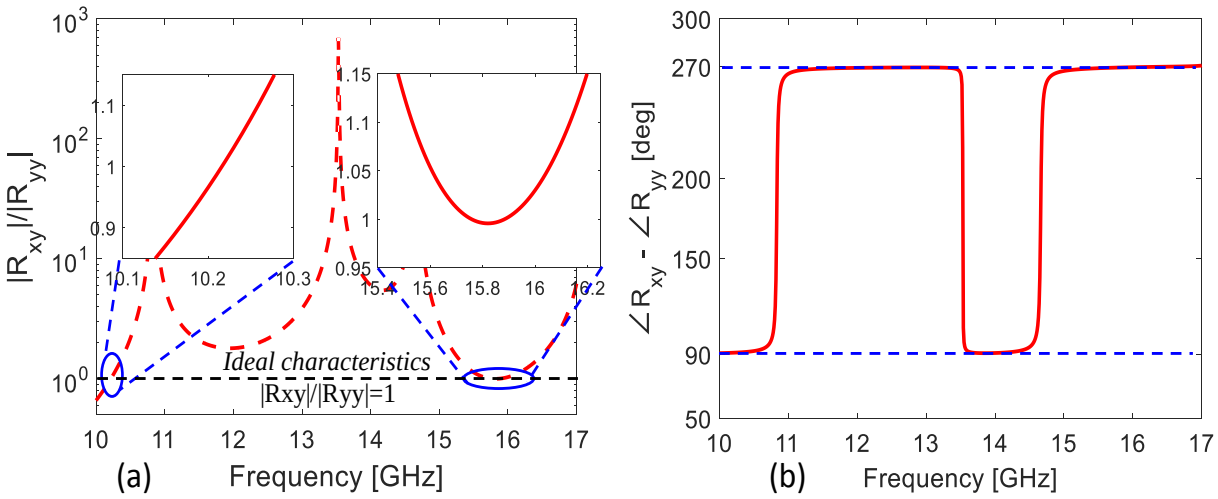

Figure 3.12: (a) Magnitude ratio of cross and co-polarized reflections. Inset shows the frequency region where metasurface exhibits ideal characteristics necessary for circular polarization. (b) Phase difference between cross and co-polarized reflections

The designed broadband cross-polarizer in Fig. 3.11(a)-(b) simultaneously provides high efficiency quarter-wave plate characteristics at multiple frequency bands. The proposed metasurface is satisfying the criteria of quarter wave plate for both magnitude ratio bandwidth which is 0.85–1.15 and phase difference bandwidth which is $90^0 \pm 5^0$ or odd multiple of 90^0.

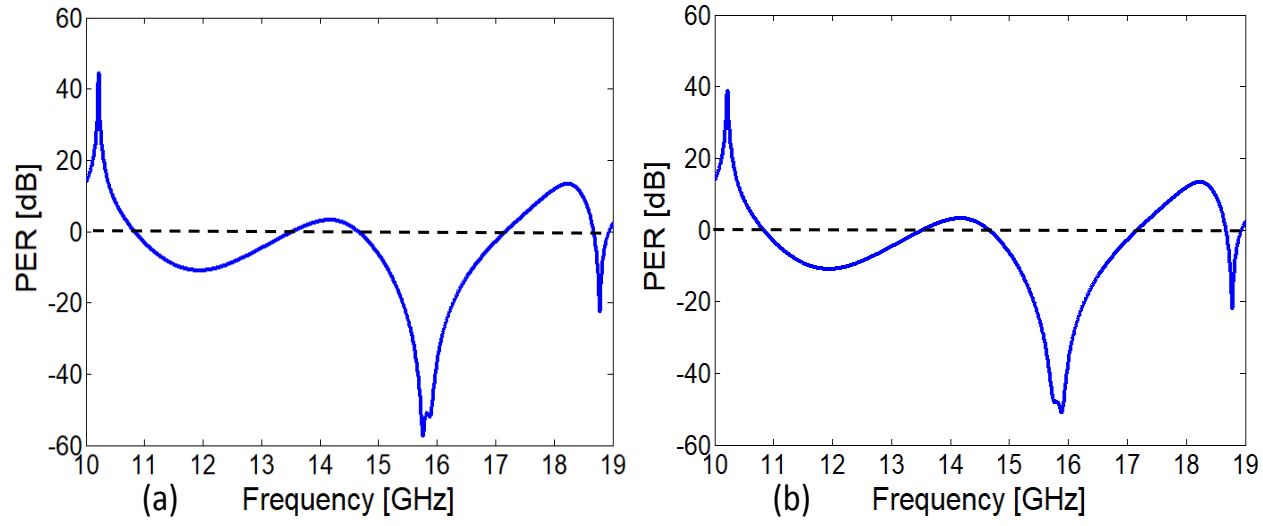

Figure 3.13: (a) Polarization extinction ratio for x-polarized incident wave (b) Polarization extinction ratio for y-polarized incident wave.

The high efficiency of circular polarization conversion can be quantified by analyzing Polarization extinction ratio (PER). It is used to characterize the handedness and efficiency of the circularly polarized wave. High efficiency RHCP or LHCP is dominating in the structure at the particular frequency or in the frequency band depends upon the small or large PER.

PER can be calculated as follows.

$$PER = 20\log_{10}\frac{|\boldsymbol{R}_{+y}|}{|\boldsymbol{R}_{-y}|} \tag{3.4}$$

Here, R_{+y} and R_{-y} are the RHCP and LHCP conversion due to y-polarized incident electric field respectively. The proposed design also gives both the LHCP and RHCP at different frequencies. It can be noted from the calculated PER in Fig. 3.13(a)-(b) that RHCP wave is dominating at 10.23 GHz where the difference of magnitude between RHCP and LHCP is nearly 40 dB. While, LHCP is dominating in the frequency band of 15.51 GHz–16.20 GHz. Difference between the magnitudes of LHCP and RHCP reaches more than 50 dB in this band which means a pure circularly polarized wave is obtained. Additionally, LHCP resonance mode obtained at 18.76 GHz but the PER efficiency is limited to -20 dB at this frequency.

The angular stability response of the quasi-crystal metasurface is also analyzed for incident angles ranging from 0^0 to 45^0. It is clear from Fig. 3.14 that if the angle of incidence changes from 0^0 to 45^0, the operating bandwidth of HWP operation remain almost stable up to 30^0 and QWP operation remain stable up to 45^0 for the first band (10.15 GHz – 10.27 GHz) while for the 2nd band (15.51 GHz – 16.20 GHz) no CP is observed above 0^0.

An additional but interesting point is that if someone looks at 45^0 incidence, i achieve five diffident bands (10.15 GHz – 10.27 GHz, 11.06 GHz – 11.54 GHz, 12.16 GHz – 12.54 GHz, 13.73 GHz – 14.07 GHz and 16.70 GHz – 16.77 GHz) where complete CP operation exists, this is only for 45^0 incidence with respect to 20dB PER bandwidth criterion.

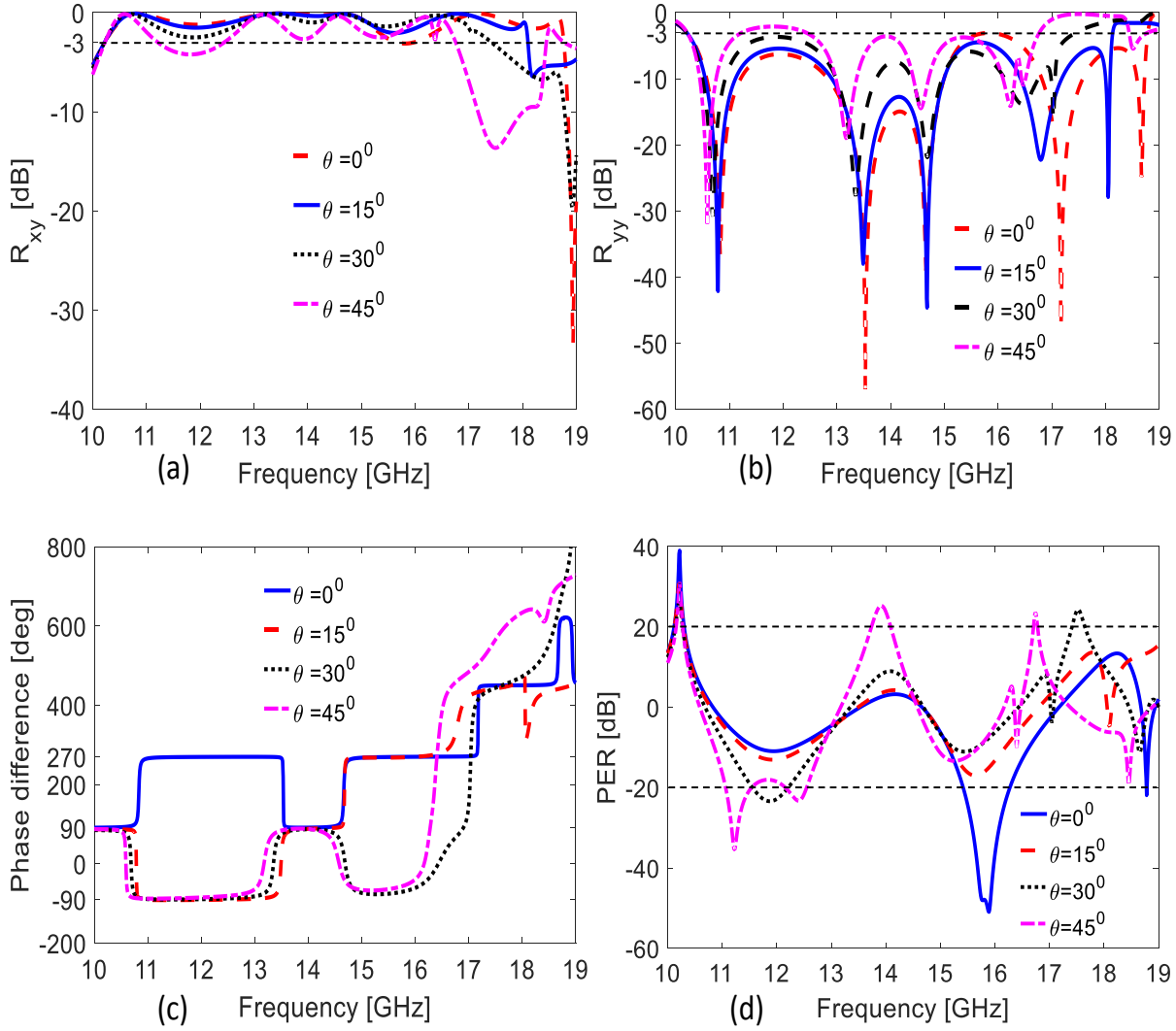

Figure 3.14: (a) Cross-polarized reflection coefficient at different incident angles (b) Co-polarized reflection coefficient (c) Phase difference between cross- and co-polarized reflections (d) PER at different angles of incoming wave.

3.3 High Efficiency Cross Polarizer

The bandwidth can also be optimized based on criterion of minimum co-polarized reflection i.e., -10 dB level. In this case, the optimized geometric parameters for small/large patches of super cell are d_1 = 1.414 mm, d_2 = 0.707 mm and r = 2.85/R = 4.2 mm. The optimized thickness of substrate h = 2 mm. In Figure 3.15(a), co-polarization reflection coefficient remains below -10 dB level supporting broadband frequency range of 10.5 GHz – 15.5 GHz.

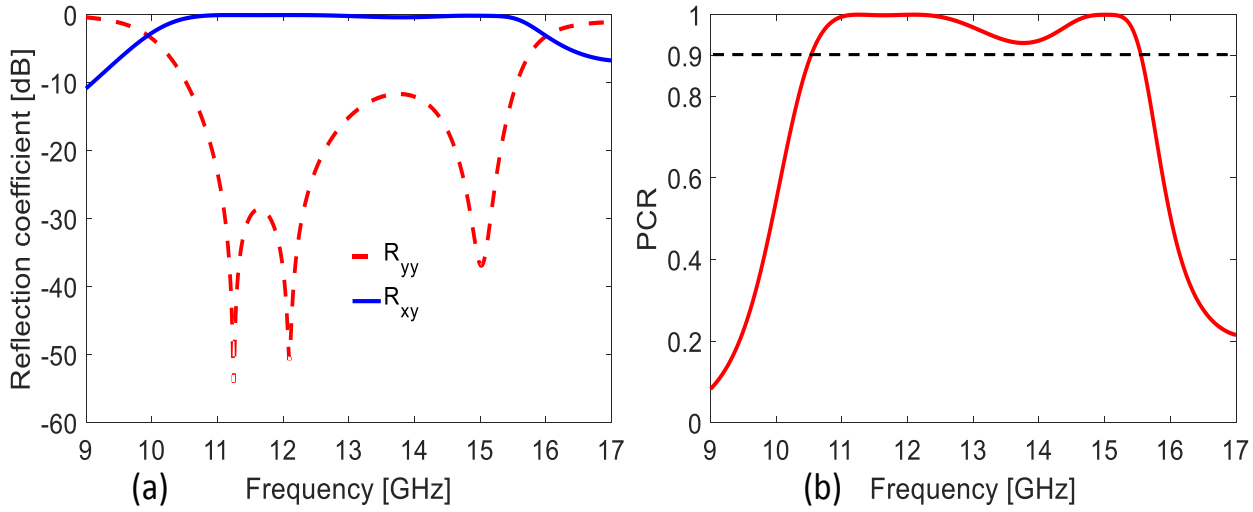

Figure 3.15: (a) High efficiency reflections for y-polarization (b) Optimized polarization conversion ratio (PCR)

The low level of co-polarization and high level of cross-polarization directly results into high efficiency of polarization conversion. Polarization conversion ratio (PCR) defines the ratio of reflected power in cross polarized component to total power in both co- and cross- polarized components.

$$PCR = \frac{|R_{xy}|^2}{|R_{yy}|^2 + |R_{xy}|^2} \tag{3.5}$$

As depicted in Fig. 3.15(b), the PCR value for the high-efficiency cross-polarizer remains above 90% within broad frequency range of 10.5 GHz – 15.5 GHz with almost 100% for the frequencies from 10.96 GHz – 12.54 GHz and 14.64 GHz – 15.29 GHz. It is pertinent to mention here that this optimized cross-polarizer also presents CP operation around 10 GHz (9.8 GHz – 10 GHz) and 16 GHz (15.89 GHz – 16.16 GHz).

3.4 Theory and Analysis

3.4.1 Structural Symmetry Analysis

To better analyze the response of the quasi-crystal structure, incident electric field along y-axis is decomposed into u- and v- components which are ±45 with respect to y-axis. It is pertinent to mention here me that the quasi-crystal metasurface exhibits mirror-symmetry around v-axis, giving same response for x- and y-polarizations. The mechanism behind cross and circular polarization can be better understood by decomposing the electric fields into u- and v-axes respectively as shown in Fig. 3.16(a). Consider E_{ui} and E_{vi} as incident electric field components in u- and v- directions respectively. The incident electric field polarized along u- and v- axes can be written as follows.

$$E_i = uE_{ui} + vE_{vi} \tag{3.6}$$

The total reflected electric field can be written as follows.

$$E_r = uR_{uu}E_{ur} + vR_{vv}E_{vr} \tag{3.7}$$

Here, R_{uu} and R_{vv} represent co-polarized reflection coefficients for u- and v- polarized incident waves respectively.

The anisotropic nature of quasi-crystal metasurface allows phase difference $\Delta\Phi$ generated between co- (R_{uu}) and cross- (R_{vv}) polarized reflection coefficients. In reality, anisotropy is the condition that causes polarization rotation. It should be noted that when the magnitude of reflection components are equal R_{uu}= R_{vv} and phase difference $\Delta\Phi$ = ±180^0, then the reflected field will be rotated along y-axis when the incident electric field is along x-axis. It is worth mentioning here, the reflected fields will be circularly polarized when the magnitude of reflection components are equal R_{uu} = R_{vv} and phase difference $\Delta\Phi$ = ±90^0.

I analyze the co-polarized reflection coefficients R_{uu} and R_{vv} for the quasi-crystal metasurface presented in Fig. 3.16. It is evident from Fig. 3.16(a) that magnitudes of both $|R_{uu}|$ and $|R_{vv}|$ are nearly 1 throughout frequency band. Fig. 3.16(b) shows that the phase difference is nearly $\Delta\Phi$ =180^0 at the five resonance frequencies. Therefore, high efficiency cross-polarization is achieved at the resonance frequencies which are in close agreement with the

Fig. 3.11. Similarly, circularly polarized reflected wave is obtained at 10.23 GHz, 15.5 GHz-16.2 GHz and 18.76 GHz because of phase difference of $\Delta\Phi = 90^0$ and 270^0 at these frequencies.

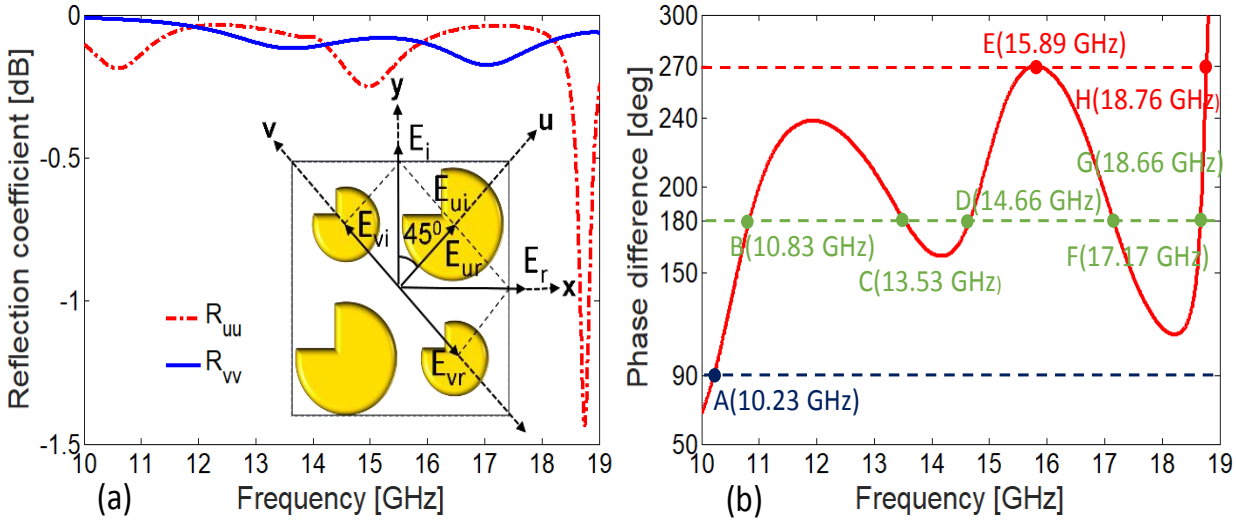

Figure 3.16: (a) Reflection coefficient for u- and v-polarized incident waves (b) Phase difference between R_{uu} and R_{vv}

3.4.2 Current Distribution Analysis

The physical mechanism of half and quarter wave plate operations can be better understood by analyzing the surface currents at the top and bottom layer of metasurface. Surface current will be induced at the top and bottom layer when y-polarized wave strikes the metasurface. The direction of surface currents on both metasurface plane and ground plane are anti-parallel to each other, see Fig. 3.17(a)-(d). According to Faraday's law, these anti-parallel induced currents at the ground layer with respect to the top layer at the resonance frequency of 10.8 GHz and 14.7 GHz will form closed current loops around the substrate resulting in induced magnetic fields (H_1, H_3) along the v-axis. x-components (H_{1x}, H_{3x}) of induced magnetic field will not cause cross polarization conversion as it is perpendicular to the incident electric field E_{iy} resulting in no cross coupling. On the other hand, y-component (H_{1y}, H_{3y}) of the induced magnetic field at the resonance frequencies is parallel to the incident electric field E_{iy} resulting in cross coupling and contributes to polarization conversion to x axis for the reflected wave.

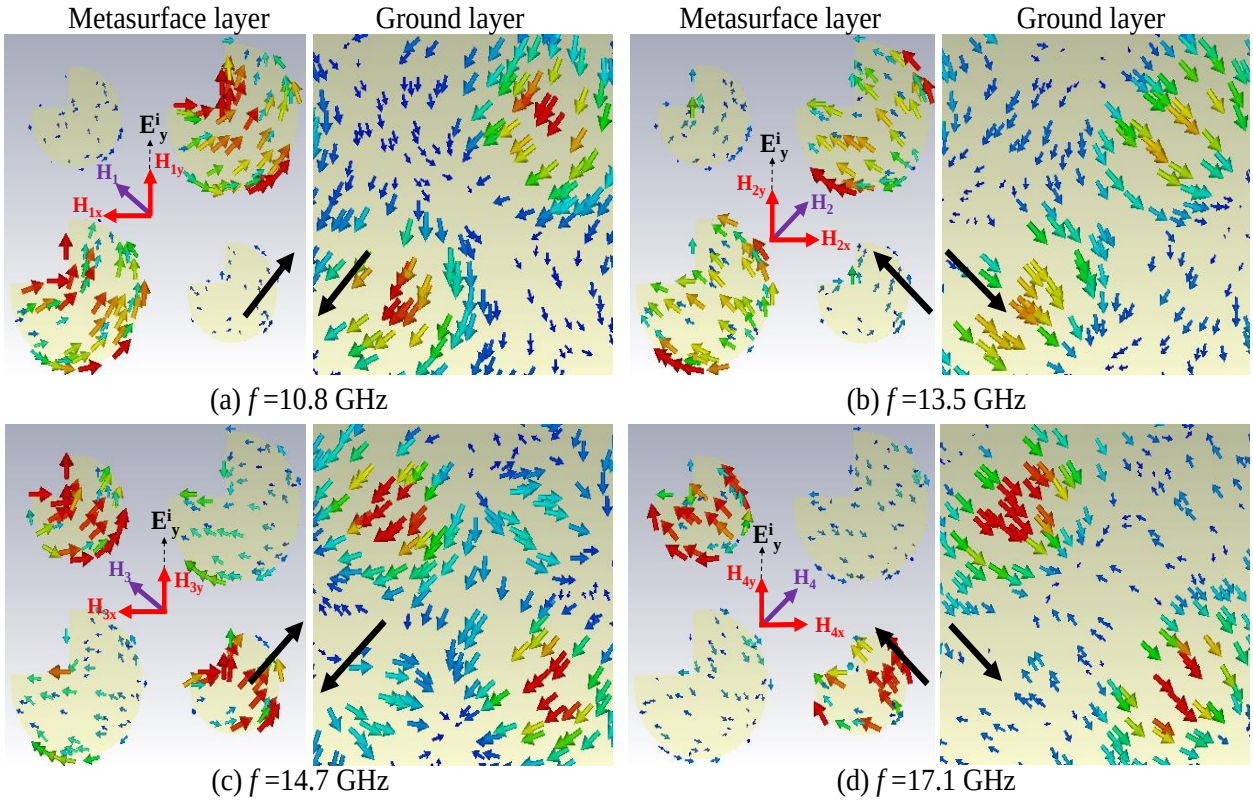

Figure 3.17: Surface current distributions on quasi-crystal metasurface on top metasurface and ground planes at four different resonance frequencies (a) 10.8 GHz (b) 13.5 GHz (c) 14.7 GHz (d) 17.1 GHz for y-polarized wave.

Similarly, for the magnetic resonance at 13.5 GHz and 17.1 GHz, the induced magnetic fields (H_2, H_4) are parallel to u-axis. Here, the direction having y-component (H_{2y}, H_{4y}) of the induced magnetic field is parallel to E_{iy} thus contributes to x-polarized reflected wave. It is interesting to note the current distributions around super cell that shows the larger patch is resonating at 10.8 GHz and 13.5 GHz and smaller patch at 14.7 GHz and 17.1 GHz respectively which is close agreement with Fig. 3.11.

3.5 Experimental Validation

To validate the simulation results, the quasi-crystal metasurface is fabricated on Rogers 5880 substrate with cross section of 305 mm × 228 mm containing 13 × 10 super cell units as shown in the inset of Fig. 3.18. The experiment was performed in fully anechoic chamber with two broadband horn antennas connected to the vector network analyzer (VNA) for the measurement of reflection coefficients as shown in Fig. 3.19. The transmitting and receiving antennas were

placed in vertical direction (y-polarized) in front of the fabricated sample to measure normally reflected co-polarized component R_{yy}. To get cross-polarized reflection R_{xy}, receiving horn antenna was rotated in horizontal direction (x-polarized).

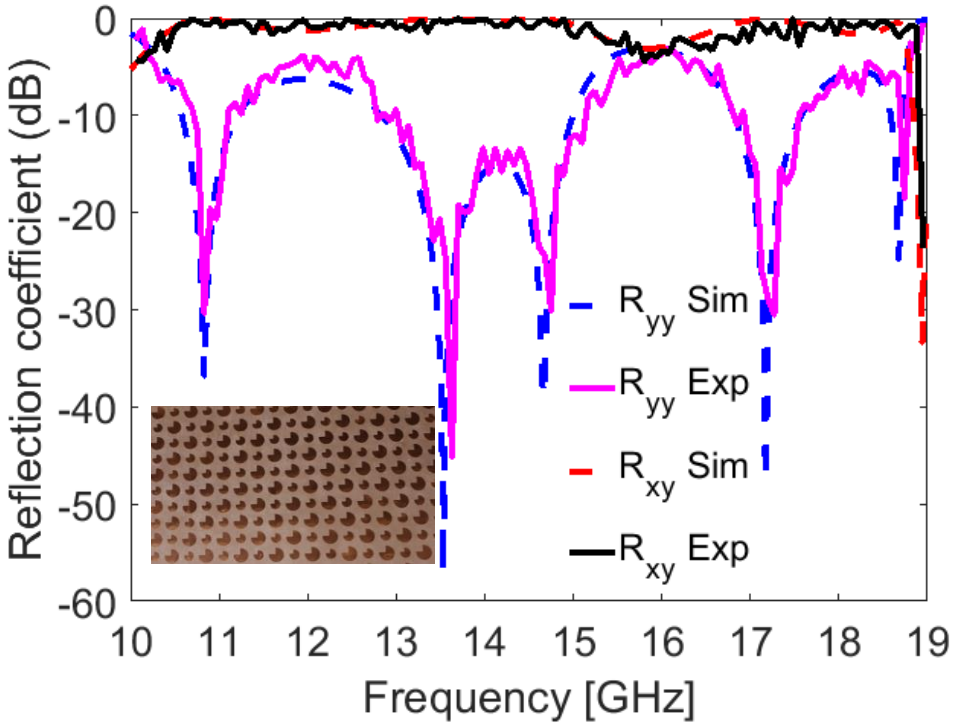

Figure 3.18: Comparison between experimental and simulation results of fabricated metasurfaces

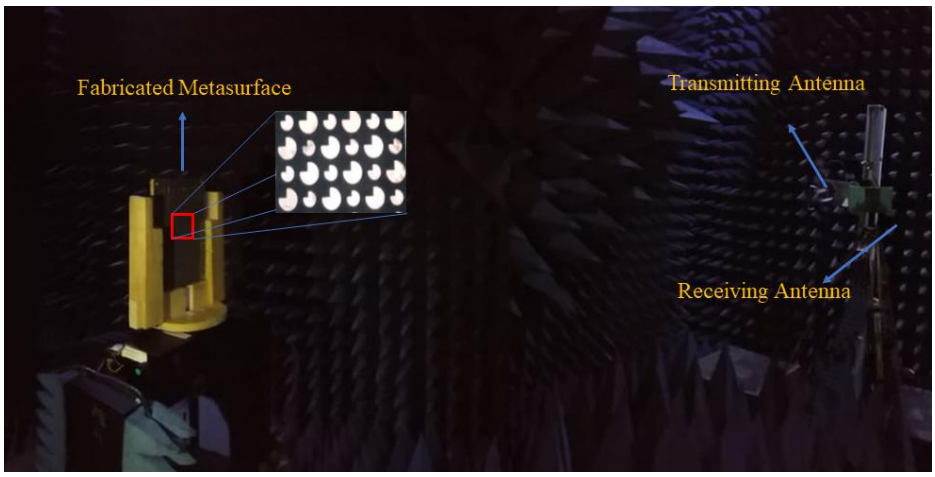

Figure 3.19: Experimental Setup in the Anechoic Chamber

Experiment was carried out for y-polarization only because of the symmetrical response of metasurface. It is clear from Fig. 3.18 that the simulation results agree well with the experimental results. However, small discrepancies arise due to misalignment of horn antennas and finite cross section of fabricated metasurface as compared to infinite periodic structure simulated in CST.

3.6 Conclusion

A quasi-crystal metasurface structure is presented in this chapter which can simultaneously work as high-efficiency dual-band cross- and circular-polarizer for wide range of frequencies under normal incidence. It is shown that the quasi-crystal metasurface is able to achieve cross-polarization (above –3 dB) at two broad ranges of frequencies between 10.28 GHz – 15.50 GHz and 16.21 GHz – 18.80 GHz. Similarly, optimized quasi-crystal metasurface is able to suppress co-polarization (below –10 dB) from 10.5 GHz – 15.5 GHz. In addition, the proposed metasurface is able to efficiently work as high efficiency circular-polarizer from 10.15 GHz – 10.27 GHz and 15.51 GHz – 16.20 GHz. Furthermore, the QWP operation of designed metasurface is also angular stable from 0^0 to 45^0 in the frequency range of 10.15 GHz – 10.27 GHz. The proposed quasi-crystal metasurface offers potential in reflect array antennas, contrast imaging, and control of radar cross-section applications etc.

CHAPTER 4

Comment on a Published Research Paper “a novel ultrathin and broadband microwave metamaterial absorber”

In this chapter, a comment on a published research paper is discussed in which original authors misinterpreted the anisotropic structure as a perfect absorber. This proclaimed metasurface is predominantly a cross polarizer for normally incident electromagnetic wave.

4.1 Introduction

Microwave metamaterial absorbers have gained significant attention in last decade since Landy *et al.* demonstrated near-unity absorption based on split-ring resonator. After that many researchers have claimed to achieve broadband absorption using metamaterial in both microwave and THz regime since metamaterial phenomenon is resonator-based, it has always been a challenge to design a perfect absorber that is broadband and polarization independent. In this and other similar anisotropic structures, the inherent unit-cell anisotropy causes flow of electric currents in the direction of lower impedances leading to the suppression of specifically polarized electric fields. Hence reflection spectrum of these polarizations would give a false impression of perfect absorption. To get total absorptivity, the receiving antennas must measure both co- and cross-polarized reflected spectra.

4.2 Unit Cell Design

In a recent article, Wang et al [51] misinterpreted an ultra-thin broadband anisotropic metamaterial structure to be absorber with absorptivity above 90% in the operating band of 8.85 GHz–14.17 GHz. The authors have neglected the cross-polarized component in their calculation of absorption. The proclaimed anisotropic pentagon patch metamaterial is predominantly a cross polarizer for the normally incident electromagnetic wave. In this

comment, the work by Wang et al. is reconsidered which is a reflective double-layer structure realized with an anisotropic pentagon patch as shown in Fig. 4.1

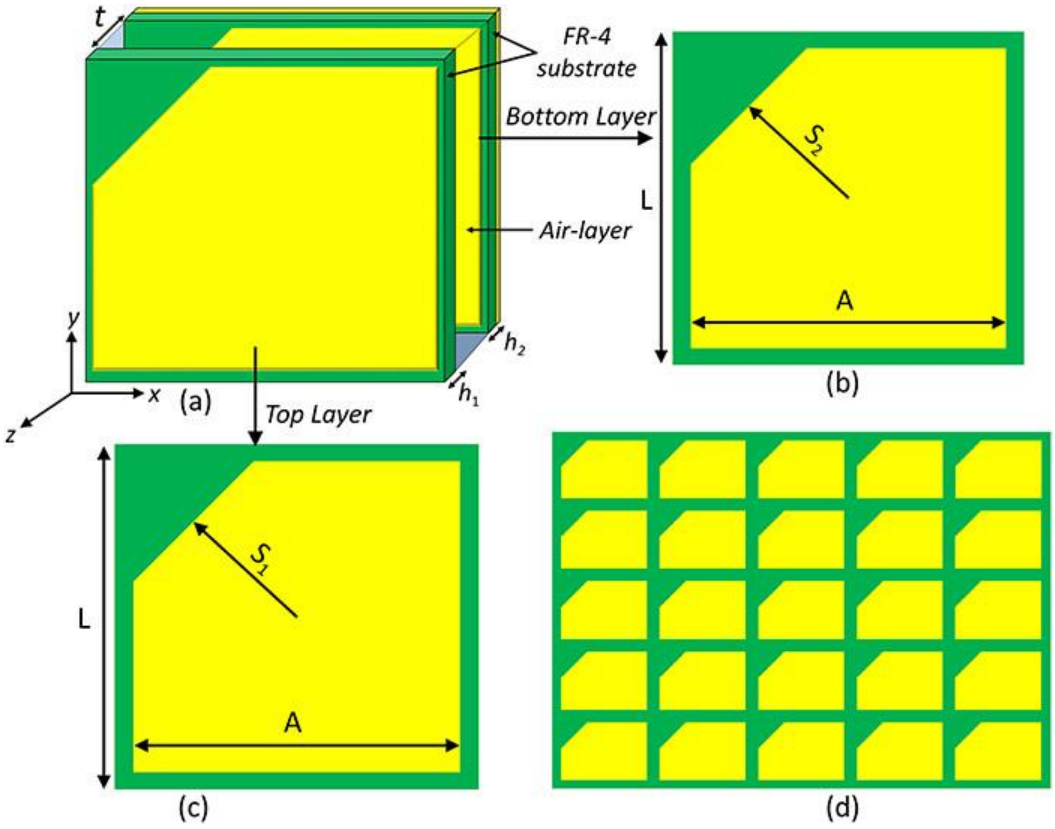

Figure 4.1: (a) Three dimensional view (b) Bottom layer (c) Top layer (d) Front view of Metasurface

4.3 Theory and Analysis

To analyze the structure, i take a heuristic approach by first resolving the pentagon unit cell into its axes of anisotropic symmetry [u- and v- axes shown in Fig. 4.2(a)] and subsequently determining the contribution of orthogonal polarization in the reflected power spectrum. Noting that the cross-polarized reflected field E_r is formed by the vector addition of the two orthogonal components E_{ru} and E_{rv}, their relation to the incident field can be related by the reflection coefficients R_{uu} and R_{vv} (defined in Fig. 4.2). To achieve a near 100 percent cross-polarization conversion, the two coefficients must be equal with unity magnitude, i.e., $|R_{uu}|=|R_{vv}|=$ 1 and ±180° phase difference, i.e., $\angle R_{uu}-\angle R_{vv}= \pm\pi$. The electric field components are numerically determined using CST Microwave studio by employing periodic

boundary conditions in x- and y-axes and Floquet port excitation in z-axis. As depicted in Figs. 4.2 (b) and (c), the near unity magnitudes of R_{uu} and R_{vv} and their nearly 180° phase difference (exactly 180° at four resonance points) in the proclaimed absorption range indicate the presence of a strong cross-polarization component. Note that some loss in magnitude results [Fig. 4.2(b)] are related to FR4 dielectric losses and copper conductivity losses.

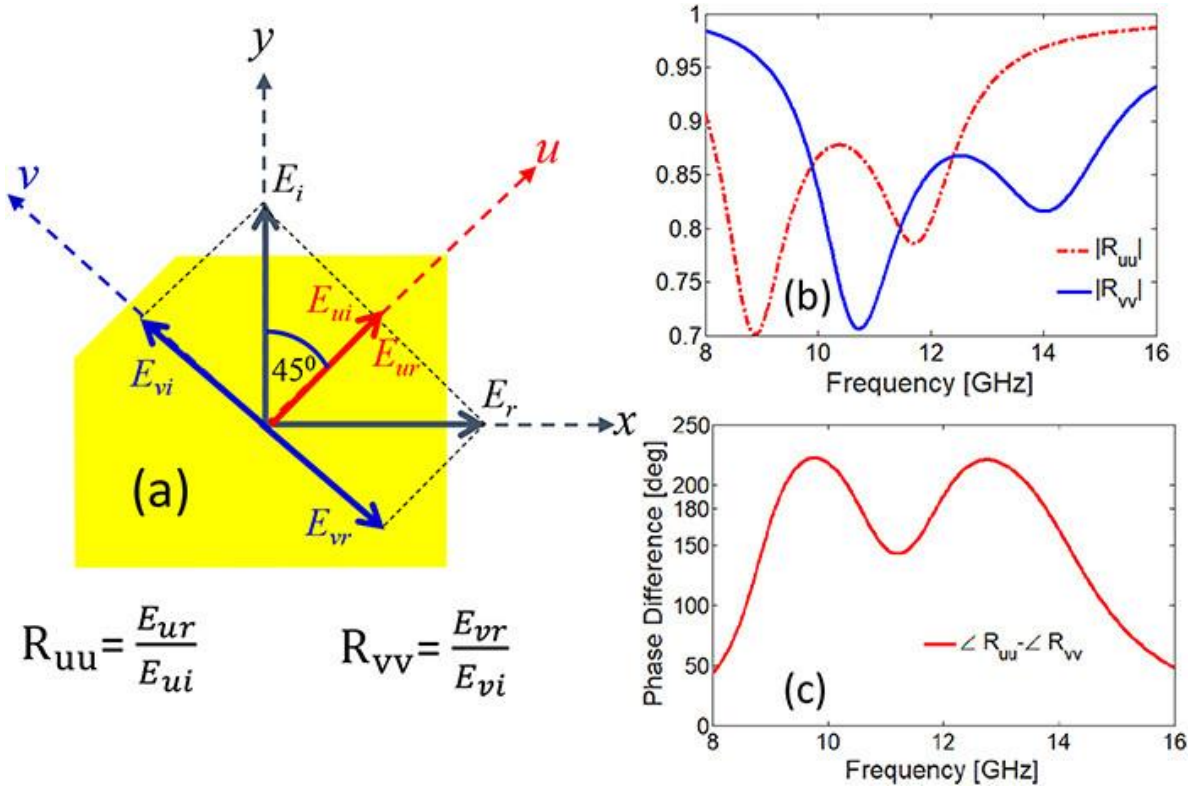

Figure 4.2: (a) Schematic illustration showing the decomposition of y- and x-axes into the axes of anisotropic symmetry (u- and v-axes) (b) The magnitude of the reflection coefficients for u- and v-polarized incident waves (R_{uu} and R_{vv}) (c) Phase difference between R_{uu} and R_{vv}

4.4 Results and Discussions

The notion of strong cross-polarized reflection is further evident when the two orthogonally directed reflection coefficients are plotted in Fig. 4.3. As shown, the dominant power in the x-polarized component of incident wave is reflected in the y-polarized component and vice versa. With the inclusion of the cross-polarized wave in Eq. (1), much less absorptivity is obtained, as depicted in the comparison of the two results in Fig. 4.4. The actual absorptivity remains below 40% over the entire spectrum, compared to 90% claimed by the authors.

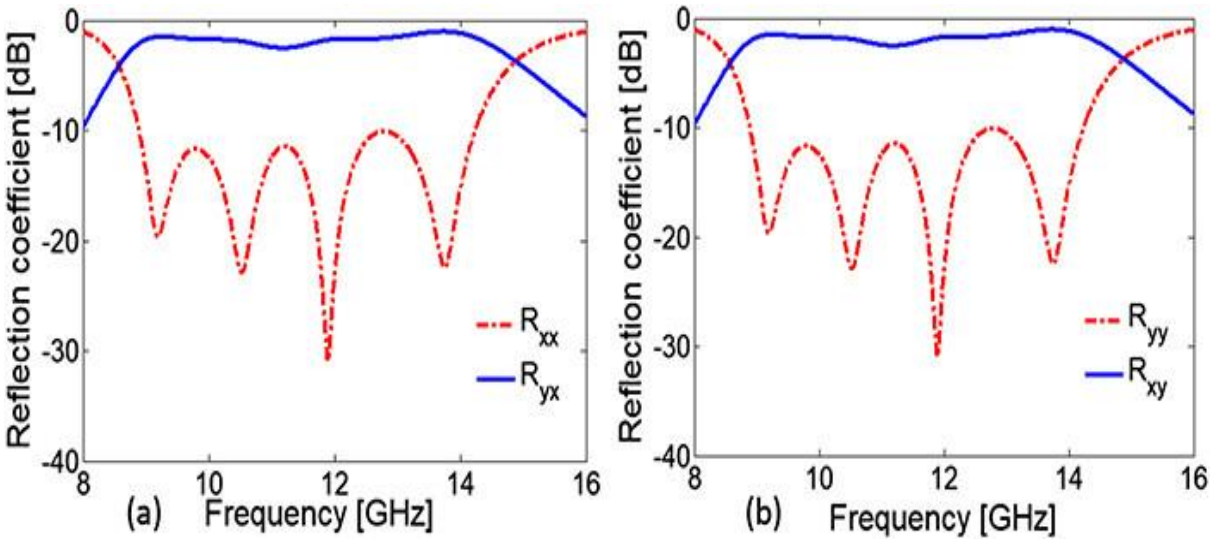

Figure 4.3: (a) Co- and cross-polarized reflections for x-polarized incident wave. (b) Co- and cross-polarized reflections for y-polarized incident wave.

The observation of an apparent perfect absorption over a wideband of frequencies was due to the fact that only co-polarized reflection coefficient (R_{ii}) was incorporated in the absorptivity expression A(ω)

$$A(\omega) = 1 - \left|R_{yy}\right|^2 + \left|R_{xy}\right|^2 - T \tag{4.1}$$

Where is the cross-polarization reflected power which was neglected by the authors and $T = |T_{yy}|^2 + |T_{xy}|^2$ is the transmission coefficient which is zero because of the presence of the metallic back-plane.

Another parameter to measure the efficiency of cross-polarizer is defined in term of polarization conversion ratio (PCR). PCR calculated from Eq.2 is above 85% in the frequency range of 8.8-14.2 GHz as shown in Fig.4.5.

$$PCR = \frac{|R_{xy}|^2}{|R_{yy}|^2 + |R_{xy}|^2} \tag{4.2}$$

Considering the PCR as shown in Fig. 4.5, this structure can be utilized for high efficiency broadband cross-polarizer applications as it converts incident electromagnetic field into its orthogonal component.

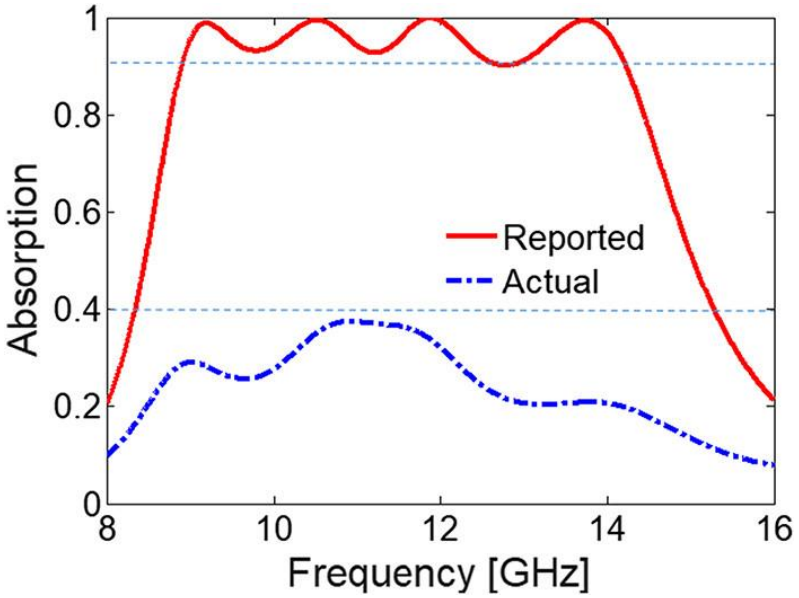

Figure 4.4: Comparison between reported and actual absorption of the designed metamaterial

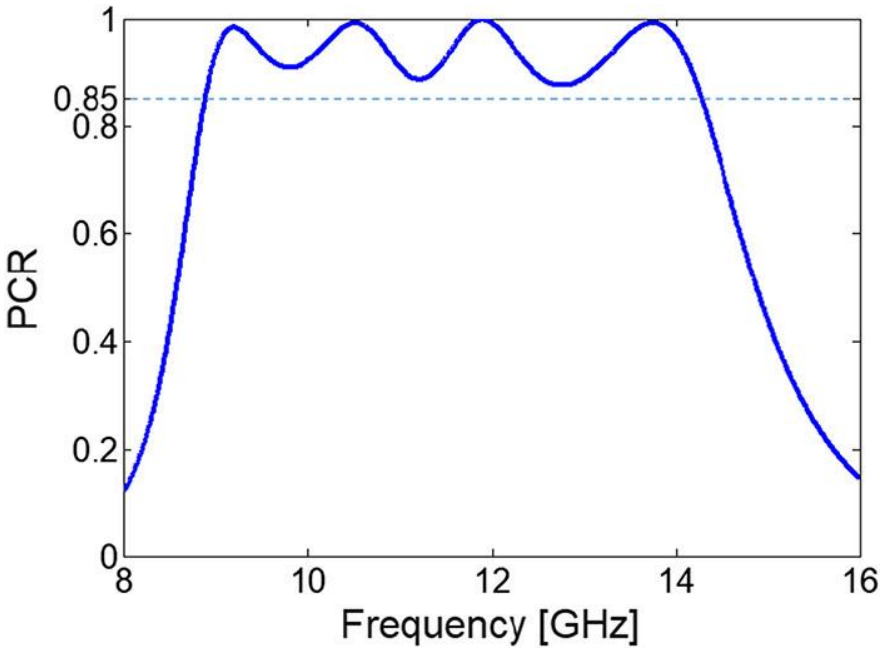

Figure 4.5: Calculated polarization conversion ratio (PCR)

4.5 Conclusion

From the above analysis, it can be concluded that Wang et al. misinterpreted the anisotropic structure as microwave absorber. The erroneous claim by the original authors was due to the ignorance of cross-component of the reflected wave. Hence, it can be deduced that the structure cannot be used for absorber applications rather it is useful for the applications where high efficiency cross-polarization is desired.

CHAPTER 5

Conclusion and Recommendations

5.1 Conclusion

In recent years, polarization control of EM waves has gained attention among researchers due to the large-scale applications. Generally, conventional techniques are used for control and manipulation of wave but have their own disadvantages. Nowadays, a lot of work is being done on metasurfaces to fill the gap created by conventional techniques. In this context, a novel technique of quasi-crystal metasurface that can simultaneously work as cross- and circular-polarizer for broad range of frequencies is simulated and experimented at microwave frequencies in this thesis. Quasi-crystal metasurface is giving high efficiency and broadband operation which is usually achieved by using multilayer structures. Although, single operation such as HWP or QWP can be achieved easily at microwave, terahertz and visible frequency regimes by employing certain type of metasurfaces. Achieving both HWP and QWP by using single layer of metasurface is itself a challenging task. In this thesis, such an ultrathin, broadband and multifunctional metasurface is designed which can help miniaturize the size of microwave and optical systems.

5.2 Recommendations

The quasi-crystal metasurface can be used in the future work as follows:

- To broaden the bandwidth of asymmetric transmission metasurfaces.
- To achieve broadband simultaneous HWP and QWP in transmission mode.
- To make dual-band or broadband power splitter at microwave frequencies.
- To achieve angular stability for multifunctional operations.
- To design perfect broadband absorbers.

REFERENCES

[1] C. A. Balanis, *Advanced engineering electromagnetics*: John Wiley & Sons, 1999.

[2] A. Gerrard and J. M. Burch, *Introduction to matrix methods in optics*: Courier Corporation, 1994.

[3] http://www.arnoldsat.com/

[4] https://electroscience.osu.edu/

[5] M. Faraday, "Faraday's Diary. Volume IV, Nov. 12, 1839-June 26, 1847," ed: George Bell and Sons, Ltd., London, 1933.

[6] E. Hecht, "Optics (2nd edn)," ed: Addisons Wesley Publications Co Inc, Waltham, 1987.

[7] N. Yu and F. Capasso, "Flat optics with designer metasurfaces," *Nature materials,* vol. 13, p. 139, 2014.

[8] S. A. Maier, M. L. Brongersma, P. G. Kik, S. Meltzer, A. A. Requicha, and H. A. Atwater, "Plasmonics—a route to nanoscale optical devices," *Advanced materials,* vol. 13, pp. 1501-1505, 2001.

[9] C. Pfeiffer and A. Grbic, "Bianisotropic metasurfaces for optimal polarization control: Analysis and synthesis," *Physical Review Applied,* vol. 2, p. 044011, 2014.

[10] J. Valentine, S. Zhang, T. Zentgraf, E. Ulin-Avila, D. A. Genov, G. Bartal, *et al.*, "Three-dimensional optical metamaterial with a negative refractive index," *nature,* vol. 455, p. 376, 2008.

[11] G. Dolling, M. Wegener, C. M. Soukoulis, and S. Linden, "Negative-index metamaterial at 780 nm wavelength," *Optics letters,* vol. 32, pp. 53-55, 2007.

[12] H.-T. Chen, W. J. Padilla, J. M. Zide, A. C. Gossard, A. J. Taylor, and R. D. Averitt, "Active terahertz metamaterial devices," *Nature,* vol. 444, p. 597, 2006.

[13] D. R. Smith, J. B. Pendry, and M. C. Wiltshire, "Metamaterials and negative refractive index," *Science,* vol. 305, pp. 788-792, 2004.

[14] V. Veselago, "VG Veselago, Sov. Phys. Usp. 10, 509 (1968)," *Sov. Phys. Usp.,* vol. 10, p. 509, 1968.

[15] J. Pendry, "JB Pendry, AJ Holden, DJ Robbins, and WJ Stewart, IEEE Trans. Microwave Theory Tech. 47, 2075 (1999)," *IEEE Trans. Microwave Theory Tech.,* vol. 47, p. 2075, 1999.

[16] R. A. Shelby, D. R. Smith, and S. Schultz, "Experimental verification of a negative index of refraction," *science,* vol. 292, pp. 77-79, 2001.

[17] N. Fang and X. Zhang, "Imaging properties of a metamaterial superlens," in *Nanotechnology, 2002. IEEE-NANO 2002. Proceedings of the 2002 2nd IEEE Conference on*, 2002, pp. 225-228.

[18] D. Schurig, J. Mock, B. Justice, S. A. Cummer, J. B. Pendry, A. Starr, *et al.*, "Metamaterial electromagnetic cloak at microwave frequencies," *Science,* vol. 314, pp. 977-980, 2006.

[19] W. Liu, Z. N. Chen, and X. Qing, "Metamaterial-based low-profile broadband mushroom antenna," *IEEE Transactions on Antennas and Propagation,* vol. 62, pp. 1165-1172, 2014.

[20] N. I. Landy, S. Sajuyigbe, J. J. Mock, D. R. Smith, and W. J. Padilla, "Perfect metamaterial absorber," *Physical review letters,* vol. 100, p. 207402, 2008.

[21] G. H. Sanders and A. Manz, "Chip-based microsystems for genomic and proteomic analysis," *TrAC Trends in Analytical Chemistry,* vol. 19, pp. 364-378, 2000.

[22] L. Huang, X. Chen, H. Mühlenbernd, H. Zhang, S. Chen, B. Bai, *et al.*, "Three-dimensional optical holography using a plasmonic metasurface," *Nature communications,* vol. 4, p. 2808, 2013.

[23] D. Lin, P. Fan, E. Hasman, and M. L. Brongersma, "Dielectric gradient metasurface optical elements," *science,* vol. 345, pp. 298-302, 2014.

[24] G. Zheng, H. Mühlenbernd, M. Kenney, G. Li, T. Zentgraf, and S. Zhang, "Metasurface holograms reaching 80% efficiency," *Nature nanotechnology,* vol. 10, p. 308, 2015.

[25] M. Kang, T. Feng, H.-T. Wang, and J. Li, "Wave front engineering from an array of thin aperture antennas," *Optics express,* vol. 20, pp. 15882-15890, 2012.

[26] C. Pfeiffer, N. K. Emani, A. M. Shaltout, A. Boltasseva, V. M. Shalaev, and A. Grbic, "Efficient light bending with isotropic metamaterial Huygens' surfaces," *Nano letters,* vol. 14, pp. 2491-2497, 2014.

[27] Y. F. Yu, A. Y. Zhu, R. Paniagua- Domínguez, Y. H. Fu, B. Luk'yanchuk, and A. I. Kuznetsov, "High- transmission dielectric metasurface with 2π phase control at visible wavelengths," *Laser & Photonics Reviews,* vol. 9, pp. 412-418, 2015.

[28] M. Amin, A. Elayouch, M. Farhat, M. Addouche, A. Khelif, and H. Bağcı, "Acoustically induced transparency using Fano resonant periodic arrays," *Journal of Applied Physics,* vol. 118, p. 164901, 2015.

[29] N. Shahid, M. Amin, S. Naureen, and S. Anand, "Mini-stop bands in single heterojunction photonic crystal waveguides," *AIP Advances,* vol. 3, p. 032136, 2013.

[30] N. Shahid, M. Amin, S. Naureen, M. Swillo, and S. Anand, "Junction-type photonic crystal waveguides for notch-and pass-band filtering," *Optics express,* vol. 19, pp. 21074-21080, 2011.

[31] J. D. Joannopoulos, S. G. Johnson, J. N. Winn, and R. D. Meade, *Photonic crystals: molding the flow of light*: Princeton university press, 2011.

[32] A. van Blaaderen, "Materials science: Quasicrystals from nanocrystals," *Nature,* vol. 461, p. 892, 2009.

[33] S. S. Kruk, C. Helgert, M. Decker, I. Staude, C. Menzel, C. Etrich, *et al.*, "Optical metamaterials with quasicrystalline symmetry: Symmetry-induced optical isotropy," *Physical Review B,* vol. 88, p. 201404, 2013.

[34] M. Amin, O. Siddiqui, M. Farhat, and A. Khelif, "A perfect Fresnel acoustic reflector implemented by a Fano-resonant metascreen," *Journal of Applied Physics,* vol. 123, p. 144502, 2018.

[35] B. Auguié and W. L. Barnes, "Collective resonances in gold nanoparticle arrays," *Physical review letters,* vol. 101, p. 143902, 2008.

[36] F. J. Garcia-Vidal, L. Martin-Moreno, T. Ebbesen, and L. Kuipers, "Light passing through subwavelength apertures," *Reviews of Modern Physics,* vol. 82, p. 729, 2010.

[37] A. D. Khan and M. Amin, "Tunable salisbury screen absorber using square lattice of plasmonic nanodisk," *Plasmonics,* vol. 12, pp. 257-262, 2017.

[38] E. R. Martins, J. Li, Y. Liu, V. Depauw, Z. Chen, J. Zhou, *et al.*, "Deterministic quasi-random nanostructures for photon control," *Nature communications,* vol. 4, p. 2665, 2013.

[39] V. G. Achanta, "Plasmonic quasicrystals," *Progress in Quantum Electronics,* vol. 39, pp. 1-23, 2015.

[40] M. Amin and A. D. Khan, "Polarization selective electromagnetic-induced transparency in the disordered plasmonic quasicrystal structure," *The Journal of Physical Chemistry C,* vol. 119, pp. 21633-21638, 2015.

[41] M. I. Khan, Q. Fraz, and F. A. Tahir, "Ultra-wideband cross polarization conversion metasurface insensitive to incidence angle," *Journal of Applied Physics,* vol. 121, p. 045103, 2017.

[42] X. Gao, X. Han, W.-P. Cao, H. O. Li, H. F. Ma, and T. J. Cui, "Ultrawideband and high-efficiency linear polarization converter based on double V-shaped metasurface," *IEEE Trans. Antennas Propag,* vol. 63, pp. 3522-3530, 2015.

[43] J. Xu, R. Li, J. Qin, S. Wang, and T. Han, "Ultra-broadband wide-angle linear polarization converter based on H-shaped metasurface," *Optics Express,* vol. 26, pp. 20913-20919, 2018/08/06 2018.

[44] Z. Wei, Y. Cao, Y. Fan, X. Yu, and H. Li, "Broadband polarization transformation via enhanced asymmetric transmission through arrays of twisted complementary split-ring resonators," *Applied Physics Letters,* vol. 99, p. 221907, 2011.

[45] K. Song, Y. Liu, C. Luo, and X. Zhao, "High-efficiency broadband and multiband cross-polarization conversion using chiral metamaterial," *Journal of Physics D: Applied Physics,* vol. 47, p. 505104, 2014.

[46] Y. Zhao, A. Qing, Y. Meng, Z. Song, and C. Lin, "Dual-band Circular Polarizer Based on Simultaneous Anisotropy and Chirality in Planar Metamaterial," *Scientific reports,* vol. 8, p. 1729, 2018.

[47] B.-Q. Lin, J.-X. Guo, B.-G. Huang, L.-B. Fang, P. Chu, and X.-W. Liu, "Wideband linear-to-circular polarization conversion realized by a transmissive anisotropic metasurface," *Chinese Physics B,* vol. 27, p. 054204, 2018.

[48] X. Gao, X.-Y. Yu, W.-P. Cao, Y.-N. Jiang, and X.-H. Yu, "Ultra-wideband circular-polarization converter with micro-split Jerusalem-cross metasurfaces," *Chinese Physics B,* vol. 25, p. 128102, 2016.

[49] X. Liu, J. Zhang, W. Li, R. Lu, L. Li, Z. Xu, *et al.*, "Three-band polarization converter based on reflective metasurface," *IEEE Antennas and Wireless Propagation Letters,* vol. 16, pp. 924-927, 2017.

[50] M. I. Khan and F. A. Tahir, "A compact half and quarter-wave plate based on bi-layer anisotropic metasurface," *Journal of Physics D: Applied Physics,* vol. 50, p. 43LT04, 2017.

[51] B.-Y. Wang, S.-B. Liu, B.-R. Bian, Z.-W. Mao, X.-C. Liu, B. Ma, *et al.*, "A novel ultrathin and broadband microwave metamaterial absorber," *Journal of Applied Physics,* vol. 116, p. 094504, 2014.

List of Publications

Journal Publications

1. **Mustafa, M.E**., Amin, M., Siddiqui, O. and Tahir, F.A., 2018. Quasi-Crystal Metasurface for Simultaneous Half-and Quarter-Wave Plate Operation. *Scientific reports*, *8*(1), pp.15743-15743.

2. **Mustafa, M.E**., Tahir, F.A., Amin, M. and Siddiqui, O., 2018. Comment on "A novel ultrathin and broadband microwave metamaterial absorber"[J. Appl. Phys. 116, 094504 (2014)]. *Journal of Applied Physics*, *124*(14), p.146101.

Conference Publications

1. **M. Mustafa**, M. S. Wahidi and F. A. Tahir, "A Broadband Linear-to-Circular Polarization Conversion Anisotropic Metasurface," *2018 18th Mediterranean Microwave Symposium (MMS)*, Istanbul, Turkey, 2018, pp. 91-93.